© 2018. Published by The Company of Biologists Ltd | Journal of Cell Science (2018) 131, jcs215517. doi:10.1242/jcs.215517

RESEARCH ARTICLE

ADAP is an upstream regulator that precedes SLP-76 at sites of TCR engagement and stabilizes signaling microclusters

Juliana B. Lewis[1,*], Frank A. Scangarello[1,2,*], Joanne M. Murphy[3], Keith P. Eidell[1], Michelle O. Sodipo[3], Michael J. Ophir[1], Ryan Sargeant[4], Maria-Cristina Seminario[3] and Stephen C. Bunnell[1,3,‡]

ABSTRACT

Antigen recognition by the T cell receptor (TCR) directs the assembly of essential signaling complexes known as SLP-76 (also known as LCP2) microclusters. Here, we show that the interaction of the adhesion and degranulation-promoting adaptor protein (ADAP; also known as FYB1) with SLP-76 enables the formation of persistent microclusters and the stabilization of T cell contacts, promotes integrin-independent adhesion and enables the upregulation of CD69. By analyzing point mutants and using a novel phospho-specific antibody, we show that Y595 is essential for normal ADAP function, that virtually all tyrosine phosphorylation of ADAP is restricted to a Y595-phosphorylated (pY595) pool, and that multivalent interactions between the SLP-76 SH2 domain and its binding sites in ADAP are required to sustain ADAP phosphorylation. Although pY595 ADAP enters SLP-76 microclusters, non-phosphorylated ADAP is enriched in protrusive actin-rich structures. The pre-positioning of ADAP at the contact sites generated by these structures favors the retention of nascent SLP-76 oligomers and their assembly into persistent microclusters. Although ADAP is frequently depicted as an effector of SLP-76, our findings reveal that ADAP acts upstream of SLP-76 to convert labile, Ca^{2+}-competent microclusters into stable adhesive junctions with enhanced signaling potential.

KEY WORDS: T cell receptor, TCR, Cellular immune response, Cytoskeleton, Cell adhesion, Cell signaling, Adaptor protein, ADAP, SLP-76, Microcluster, Confocal microscopy

INTRODUCTION

The signals initiated in response to T cell antigen receptor (TCR) ligation are mediated by macromolecular complexes known as ‘microclusters’. These complexes incorporate the TCR, the receptor-associated tyrosine kinase ZAP-70, and a wide range of signaling proteins with crucial roles in T cell development and activation. Microclusters play a decisive role in T cell activation, as multiple signals and morphological changes are triggered in response to the formation of a single microcluster (Bunnell et al., 2001, 2002; Huse et al., 2007). Given the small sizes of the TCR and its cognate ligands, the glycocalyx presents a significant steric barrier to TCR engagement. This barrier is actively overcome by dynamic actin-rich protrusive structures that continuously explore the stimulatory surface, generating the closely apposed domains required for TCR engagement (Seminario and Bunnell, 2008; Bunnell, 2010; Cai et al., 2017). Microclusters preferentially form at the sites where the tips of these structures encounter ligand-bearing surfaces. Within a few moments of the formation of an individual microcluster, a dramatic increase in actin polymerization drives the advancement of the T cell over the stimulatory substrate, favoring the development of additional contacts and microclusters. These microclusters are actively transported towards, and terminated within, the central domain of the immune synapse, explaining the fact that continuous antigen recognition is required for efficient T cell activation (Valitutti et al., 1995; Varma et al., 2006; Vardhana et al., 2010).

The adaptor proteins LAT and SLP-76 (also known as LCP2) are both tyrosine phosphorylated by ZAP-70 and are essential hubs for the recruitment of SH2 domain-containing signaling proteins, including Gads (also known as GRAP2), Grb2, PLCγ1 and Vav1 (Bunnell et al., 2002, 2006; Braiman et al., 2006; Houtman et al., 2006; Nguyen et al., 2008; Sylvain et al., 2011). These proteins are initially assembled into microclusters at sites of TCR engagement and ZAP-70 recruitment, but gradually segregate into distinct signaling complexes known as ‘SLP-76 microclusters’. These structures are subjected to centripetal forces that, if the stimulatory ligand is immobile, detach these complexes from the TCR and transport them to the center of the stimulatory interface. Even though these structures are stabilized by an extensive network of interactions among their constituent proteins, they gradually dissipate following their separation from the TCR. Perturbations that reduce the persistence of SLP-76 microclusters reduce T cell activation, and vice versa, suggesting that these processes are causally linked (see discussion in Sylvain et al., 2011).

SLP-76 serves as a bridge from LAT to downstream effectors, such as PLCγ1 and Vav1, which are integral to the LAT-dependent core of SLP-76 microclusters (Sherman et al., 2016). This function requires the recruitment of SLP-76 to LAT via the SH2 domain-containing adaptor protein Gads, the phosphorylation of SLP-76 by ZAP-70, and the subsequent recruitment of effector proteins via tyrosine phosphorylation sites in the N-terminus of SLP-76. While early studies suggested that the C-terminal SLP-76 SH2 domain was dispensable for T cell activation, the inactivation of this domain inhibits TCR-induced proliferation and S-phase entry as potently as the inactivation of the Gads binding site in SLP-76 (Boerth et al., 2000; Myung et al., 2001). Subsequent studies revealed that the SLP-76 SH2 domain also contributes to TCR-induced adhesion to integrin ligands, to the positive and negative selection of thymocytes, and to TCR-induced cytoskeletal

[1]Program in Immunology, Sackler School of Graduate Biomedical Sciences, Tufts University School of Medicine, Boston, MA 02111, USA. [2]Medical Scientist Training Program, Sackler School of Graduate Biomedical Sciences, Tufts University School of Medicine, Boston, MA 02111, USA. [3]Department of Immunology, Tufts University School of Medicine, Boston, MA 02111, USA. [4]Pacific Immunology Corporation, Ramona, CA 92065, USA.
*These authors contributed equally to this work

‡Author for correspondence (stephen.bunnell@tufts.edu)

J.B.L., 0000-0001-6679-2002; F.A.S., 0000-0002-3993-608X; J.M.M., 0000-0001-7542-4690; K.P.E., 0000-0002-5971-218X; M.O.S., 0000-0001-5001-7298; M. J.O., 0000-0002-5516-1237; M.-C.S., 0000-0003-0762-8661; S.C.B., 0000-0001-6887-0828

Received 17 January 2018; Accepted 17 September 2018

Journal of Cell Science (2018) 131, jcs215517. doi:10.1242/jcs.215517

rearrangements (Baker et al., 2009; Burns et al., 2011; Pauker et al., 2011). However, the precise contribution of the SLP-76 SH2 domain to microcluster assembly and persistence remains controversial (Bunnell et al., 2006; Baker et al., 2009; Pauker et al., 2011; Coussens et al., 2013).

The two best-characterized ligands of the SLP-76 SH2 domain are the adhesion and degranulation-promoting adaptor protein (ADAP; also known as FYB1) and the serine/threonine kinase hematopoietic progenitor kinase-1 (HPK1; also known as MAP4K1). However, the signaling and pro-adhesive functions attributed to the adaptor ADAP best correspond to the abnormalities observed in the absence of a functional SLP-76 SH2 domain (Griffiths et al., 2001; Peterson et al., 2001; Wang et al., 2004, 2009; Kliche et al., 2006, 2012; Wu et al., 2006; Medeiros et al., 2007; Burbach et al., 2008; Srivastava et al., 2010; Sylvester et al., 2010; Pauker et al., 2011; Mitchell et al., 2013). By contrast, HPK1 phosphorylates microcluster components in a manner that leads to their ubiquitylation and degradation (di Bartolo et al., 2007; Shui et al., 2007; Patzak et al., 2010; Lasserre et al., 2011). Consistent with these findings, ADAP and its associated adaptor protein SKAP55 (also known as SKAP1), co-migrate with SLP-76 in microclusters, while HPK1 actively destabilizes SLP-76 microclusters (Pauker et al., 2011; Coussens et al., 2013; Ophir et al., 2013). Although ADAP has typically been depicted as a downstream effector of SLP-76, no previous studies have considered how ADAP is phosphorylated prior to its interaction with the SH2 domain of SLP-76 (Peterson, 2003; Rudd and Wang, 2003; Acuto et al., 2008).

Here, we show that the interaction of ADAP with SLP-76 enhances the cohesion, persistence and movement of TCR-induced SLP-76 microclusters, promotes the formation of stable T cell contacts and strengthens the integrin-independent adhesive junctions formed by the TCR. These functions of ADAP require the three known SLP-76-interacting tyrosine residues: Y595, Y651 and Y771. By using a novel ADAP phosphorylation-site specific antiserum, we show that a SLP-76-interacting residue within ADAP, Y595, is acutely phosphorylated in response to TCR ligation, and that virtually all ADAP phosphorylation occurs within the pool of ADAP that is phosphorylated on Y595. Our data support a model in which cooperative interactions with SLP-76 preferentially protect multiply phosphorylated ADAP molecules from de-phosphorylation. By overexpressing a C-terminal fragment of ADAP, we establish that the N-terminal portion of ADAP facilitates Y595 phosphorylation and is crucial for the maintenance of SLP-76 microclusters. Strikingly, phosphorylated ADAP occurs within SLP-76 microclusters, while non-phosphorylated ADAP is enriched at the tips of protrusive actin-rich structures, where microclusters first form in response to TCR engagement. Finally, cytoskeletal structures transiently deliver ADAP to TCR contact sites in advance of SLP-76, even in the absence of a functional SLP-76 SH2 domain. These data suggest a substantially revised model of T cell activation, in which dynamic cytoskeletal rearrangements deliver ADAP to nascent contact sites, where phosphorylated ADAP fosters the retention of SLP-76 oligomers within persistent signaling microclusters.

RESULTS

The SH2 domain of SLP-76 is required for microcluster persistence and movement

SLP-76 consists of a pro-oligomeric sterile α motif (SAM), a tyrosine phosphorylatable effector-binding domain (YYY), a proline-rich linker containing a Gads-binding site (G2), and a C-terminal SH2 domain (Fig. 1A) (Liu et al., 2013). As the SH2 domain of SLP-76 impacts on the number, area and intensity of SLP-76 microclusters, the developmental and functional consequences of inactivating the SLP-76 SH2 domain may stem from changes in microcluster function (Myung et al., 2001; Bunnell et al., 2006; Burns et al., 2011; Pauker et al., 2011; Coussens et al., 2013). However, the impact of the SLP-76 SH2 domain on the dynamic behavior of SLP-76 microclusters has been more controversial, with studies reporting either complete ablation or their conversion into short-lived clusters that move randomly (Bunnell et al., 2006; Pauker et al., 2011). To eliminate potential sources of discrepancy, we generated identically tagged chimeras of human and murine SLP-76 (2xHA.SLP-76.YFP) and performed detailed quantitative analyses of SLP-76 microcluster persistence and movement in J14 cells acutely transfected with matched levels of these wild-type (WT) or SH2 mutant (R448K; 'RK') chimeras (Table S1). Following stimulation on antibody-coated glass coverslips, WT SLP-76 formed persistent and mobile SLP-76 microclusters, whereas the SLP-76 RK mutant formed microclusters that were fewer in number, less persistent, less mobile and recruited a smaller fraction of the available SLP-76 (Fig. 1B,C; Table S1; Movies 1,2). The behaviors of human and murine chimeras were statistically indistinguishable; thus, our earlier report (Bunnell et al., 2006) may have been influenced by tagging strategies or by long-term adaptations within stable cell lines.

The SH2 domain of SLP-76 enables microcluster cohesion

The mode of microcluster dissociation differs markedly in the absence of a functional SH2 domain. WT SLP-76 microclusters rapidly increased in size and, after a brief lag, moved *en bloc* toward the center of the contact, dissipating gradually (Movies 3,4). In contrast, RK mutant SLP-76 microclusters continuously shed smaller structures containing SLP-76 (Movies 5,6). These structures were dim, moved rapidly, and either dissipated or moved out of the focal plane within seconds. These particles did not show the bias towards centralization displayed by the WT SLP-76 microclusters. To de-emphasize regions of constant cytoplasmic background, we made images of the standard deviation of image intensity over time (Fig. 1D). These images accentuate the sites at which WT microclusters are nucleated and reveal the average trajectories of microclusters departing these sites. While the sites at which RK mutant microclusters formed are accentuated, the numerous small particles departing these sites created diffuse 'clouds'. Thus, an intact SLP-76 SH2 domain is required for the cohesion and directional transport of SLP-76 microclusters.

The SLP-76 SH2 domain promotes contact stability and T cell adhesion

In fixed cells, the perturbation of the SLP-76 SH2 domain alters the organization of the actin cytoskeleton, reducing the radial symmetry of the cell contact at the stimulatory interface (Pauker et al., 2011). In live-cell studies, we observed that parental J14 cells typically failed to spread after contacting stimulatory substrates, while J14 cells reconstituted with a WT SLP-76 chimera rapidly generated symmetric contacts bounded by stable, compact lamellipodia. In contrast, J14 cells reconstituted with matched levels of the SH2 domain mutant (RK) chimera responded to the substrate by generating larger lamellipodia that fluctuated over time. Manual scoring by researchers who were blind to the condition validated these differences (Fig. 1E; see Fig. S1A for examples). We also quantified the expansion and retraction of cell boundaries over time, as described previously. This approach confirmed that WT, but not RK mutant, SLP-76 reduced the fluctuation of the contact boundary

Journal of Cell Science (2018) 131, jcs215517. doi:10.1242/jcs.215517

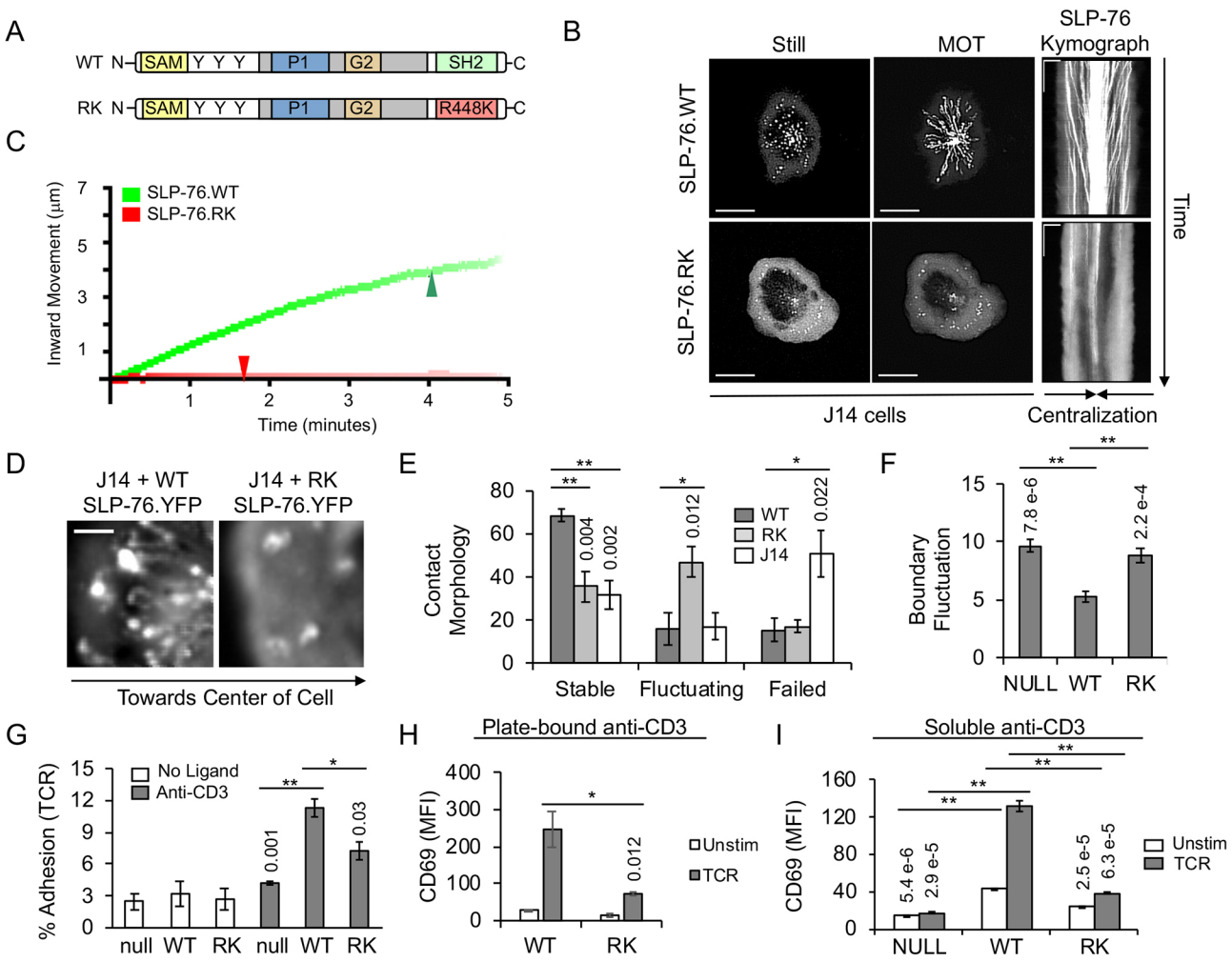

Fig. 1. The SLP-76 SH2 domain regulates microcluster integrity and cell adhesion. (A) Domain structures of SLP-76.YFP chimeras. (B) SLP-76-deficient (J14) cells expressing human SLP-76.YFP were stimulated on OKT3-coated glass coverslips and imaged for 5 min after contacting the stimulatory substrate. Representative still (left) and maximum over time (MOT, center) images are shown. Scale bars: 10 µm. In MOT images, persistent and mobile SLP-76 microclusters generate radial traces (n=6 experiments; 46 WT cells, 45 RK cells). Kymographs (right) depicting movement in a narrow region spanning the cell diameter over time. Scale bars: 5 µm, horizontal; 60 s, vertical. (C) For the conditions in B, SLP-76 microcluster trajectories were manually traced in iVision and average trajectories are shown as composite kymographs. The x- and y-axes depict centripetal displacement over time and intensity encodes the fraction of clusters persisting; arrowheads indicate the time at which half of the microclusters had dissociated. Microcluster properties, number of cells analyzed and statistical comparisons are listed in Table S1. (D) Regions of cells imaged in B are shown as 'standard deviation over time' images. Scale bar: 1 µm. Areas showing a dramatic change over time appear brightest white, as occurs when bright clusters move through a dark field. Lines indicate movement over time. (E) Contact morphology of transiently transfected J14 cells, stimulated as in B. The percentage of cells falling in each category is shown (n=6 experiments; WT, 176 cells; RK, 217 cells; parental J14, 85 cells). (F) Boundary fluctuation values correspond to the areas undergoing retraction or expansion over a 30 s window, expressed as a percentage of the initial cell area (n=3 experiments; WT, 10 cells; RK, 11 cells; parental J14, 8 cells). (G) TCR adhesion assays were performed in J14 cells stably expressing matched levels of the indicated SLP-76.YFP chimeras. Fractional cell retention on OKT3 is shown (n=3 experiments). (H) J14 cells stably transduced with SLP-76.mYFP chimeras were assayed for TCR-induced CD69 upregulation using plate-bound OKT3 (n=3 experiments). (I) J14 cells transiently expressing mYFP chimeras were assayed for TCR-induced CD69 upregulation using soluble OKT3 (n=3 experiments). All errors are displayed as s.e.m. *P<0.05; **P<0.01 compared with J14 cells expressing WT SLP-76.YFP (Student's two-tailed t-test for unpaired samples).

in J14 cells (Fig. 1F; see Fig. S1B for examples). As in our previous study, the ability to maintain a stable contact boundary correlated with the ability of T cells to resist detachment from stimulatory substrates bearing TCR ligands (Fig. 1G; Ophir et al., 2013). Jointly, these data suggest that the SH2 domain of SLP-76 contributes to the assembly of TCR-dependent adhesive structures and the maintenance of a stable and symmetric contact.

The SLP-76 SH2 domain is differentially involved in TCR-dependent signaling pathways

Although we previously reported that the SH2 domain contributes to TCR-dependent NF-AT activation and CD69 upregulation, these studies were performed in a stable cell line that failed to generate any SLP-76 microclusters (Bunnell et al., 2006). Revisiting these phenomena in transiently transfected J14 cells, we observed that the labile clusters formed by the SH2 domain-inactivated (RK) SLP-76 chimera were associated with a statistically non-significant decline in TCR-induced Ca^{2+} entry in response to soluble TCR ligands (Fig. S1C) and a dramatic reduction in the upregulation of CD69 with both plate-bound and soluble TCR ligands (Fig. 1H,I). While our Ca^{2+} data conflict with a more recent study that examined the responses triggered by low-dose TCR ligation (Coussens et al., 2013), normal Ca^{2+} function has also been observed in primary T cells bearing an identical mutation in the SLP-76 SH2 domain

Journal of Cell Science (2018) 131, jcs215517. doi:10.1242/jcs.215517

(Myung et al., 2001; Burns et al., 2011). Consistent with these findings, J14 cells stably transduced with the SLP-76 RK mutant maintained normal levels of phosphorylated PLCγ1 and ERK1/2 following stimulation with soluble antibodies (Fig. S1D). Thus, the labile microclusters produced in the absence of a functional SLP-76 SH2 domain support cytoplasmic Ca^{2+} elevations, PLCγ1 phosphorylation and ERK1 activation, but are insufficient to drive optimal CD69 upregulation.

ADAP-120 and ADAP-130 are recruited into TCR-induced microclusters

The adaptor ADAP is one of the best-characterized ligands of the SLP-76 SH2 domain. ADAP consists of an N-terminal proline-rich region and a C-terminal region that contains two atypical 'helically extended' SH3 (hSH3) domains (Fig. S2A). The former region contains a constitutive binding site for the SH3 domain of the adaptor SKAP55, and the hSH3 domains of the latter region are flanked by multiple tyrosine phosphorylation sites, including the SLP-76 SH2 domain-binding tyrosine residues 595, 651 and 771 (Geng et al., 1999; Raab et al., 1999; Lange et al., 2010; Sylvester et al., 2010; Pauker et al., 2011; Coussens et al., 2013). In addition to the well-characterized ADAP-120 isoform, alternative splicing generates the longer ADAP-130 isoform, which incorporates an exon between the SLP-76-binding sites at Y595 and Y651 (Fig. S2A) (Veale et al., 1999). Although ADAP-120 is preferentially expressed during thymic development and in Jurkat T cells, while ADAP-130 predominates in peripheral T cells, ADAP-130 has never been visualized in live cells. To determine whether the altered spacing of the SLP-76-binding sites in ADAP influences microcluster behavior, J14 cells stably reconstituted with SLP-76.YFP (J14.SY cells) were transiently transfected with ADAP chimeras tagged at the N-terminus with a 3×Flag-tagged version of TagRFP-Turbo (3×Flag.TRT). In response to immobilized TCR ligands, both isoforms of ADAP entered persistent SLP-76 microclusters that moved towards and accumulated in the center of the contact (Fig. S2B; Movies 7–9). Although some cell-to-cell variability was noted, neither isoform altered the dynamic behavior of TCR-induced SLP-76 microclusters when overexpressed (Fig. S2C; Table S2). Despite reports suggesting that the hSH3 domains of ADAP interact with acidic phospholipids, we did not observe any recruitment of ADAP to the plasma membrane outside of SLP-76 microclusters (Heuer et al., 2005, 2006).

ADAP supports TCR-dependent contact formation and microcluster persistence

To more carefully quantify the contributions of ADAP to microcluster stability and movement, we performed overexpression and knockdown-addback studies in transiently transfected J14.SY cells. Under these conditions, the knockdown vector eliminated endogenous ADAP, while the knockdown-addback vector yielded levels of exogenous ADAP comparable to those of endogenous ADAP in unmanipulated cells (Fig. 2A). When plated on stimulatory coverslips, ADAP-knockdown cells generated fewer well-spread contacts than the parental J14.SY cells or the reconstituted knockdown-addback cells, confirming that ADAP plays an important role in contact morphology (Fig. 2B,C; Pauker et al., 2011). The overexpression of ADAP-120 did not alter the fundamental properties of SLP-76 microclusters (Fig. 2D,E; Fig. S2B,C, Table S2). However, in the absence of ADAP, TCR-induced SLP-76 microclusters were dimmer, less persistent and immobile, as observed with the SH2 mutant of SLP-76 (Fig. 2D,E; Movie 10). ADAP-120 re-expression confirmed that these changes were specifically caused by the loss of ADAP (Fig. 2D,E; Movie 11). In addition, standard deviation over time analyses demonstrated that the SLP-76 microclusters observed in the absence of ADAP exhibited defects in microcluster cohesion comparable to those observed in J14 cells expressing the SLP-76 SH2 domain mutant (Fig. 2F). These data confirm that ADAP promotes the formation of cohesive, persistent and mobile microclusters, enhances contact symmetry, and favors adhesion via the TCR.

Y595 and Y651 govern the entry of ADAP into SLP-76 microclusters

In fixed cells, the overexpression of ADAP mutants affecting any of the SLP-76-binding tyrosine residues (Y595, Y651 and Y771) attenuated the recruitment of SLP-76 into microclusters. Similarly, the Y595F/Y651F double mutant reduced the persistence of SLP-76 microclusters (Coussens et al., 2013). In related studies, we confirmed that the overexpression of either the Y595F or Y595F/Y651F (2YF) mutant of ADAP reduced the fraction of SLP-76 in microclusters, as well as the microcluster lifetime, the total microcluster displacement, and the speed of microcluster movement (Fig. S2B,D; Table S2). To clarify the functions of these tyrosine residues in the absence of endogenous ADAP, we also examined the behaviors of ADAP and SLP-76 in live ADAP-deficient Jurkat T cells (JDAP cells) transiently reconstituted with ADAP mutants (Fig. 3A) (Huang et al., 2005). As in Fig. 2, the absence of ADAP caused SLP-76 to assemble into dim, labile microclusters that did not centralize (Fig. 3B,C, null; Table S3). Expression of WT ADAP led to normal SLP-76 clustering and dynamics. Even though the ADAP Y595F mutant retains Y651 and Y771, the Y595F mutant had virtually no positive impact on microcluster movement and stoichiometry, a limited effect on microcluster persistence, and was only transiently observed in SLP-76 microclusters. Similar defects were observed in cells expressing the Y595F/Y651F double mutant (2YF), which entered SLP-76 microclusters even less well than the Y595F mutant. Finally, the expression of the ADAP Y595F/Y625F/Y651F triple mutant (3YF), which incorporates a mutation in the Fyn SH2 domain binding site, did not rescue the persistence, movement or stoichiometry of SLP-76 microclusters. Taken together with data from previous reports, these data confirm that multivalent interactions involving both Y595 and Y651 are required to link ADAP with SLP-76.

ADAP Y595 is acutely phosphorylated in response to TCR stimulation

The mechanisms responsible for the phosphorylation of ADAP prior to its interaction with SLP-76 remain unclear. Here, we verified that ADAP and its constitutive binding partner SKAP55 are acutely tyrosine phosphorylated following TCR ligation (Fig. S3A). Because the Y595F mutation profoundly impaired the persistence and movement of SLP-76 microclusters, we generated an affinity-purified antiserum targeting phosphorylated Y595 (pY595) using the phospho-peptide indicated in Fig. S3B (boxed). TCR-induced Y595 phosphorylation of endogenous ADAP peaked within 5 min and was undetectable in ADAP-deficient control cells (Fig. S3C). Given the similarity of the SLP-76 SH2 domain-binding sites at Y595, Y651 and Y771, the pY595 antiserum was remarkably selective, and displayed minimal cross-reactivity towards an exogenously expressed ADAP Y595F mutant (Fig. S3D). Finally, consistent with previous *in vitro* studies that demonstrated that ADAP could be phosphorylated by Fyn, the Src-family kinase inhibitor PP2 blocked the TCR-induced phosphorylation

Journal of Cell Science (2018) 131, jcs215517. doi:10.1242/jcs.215517

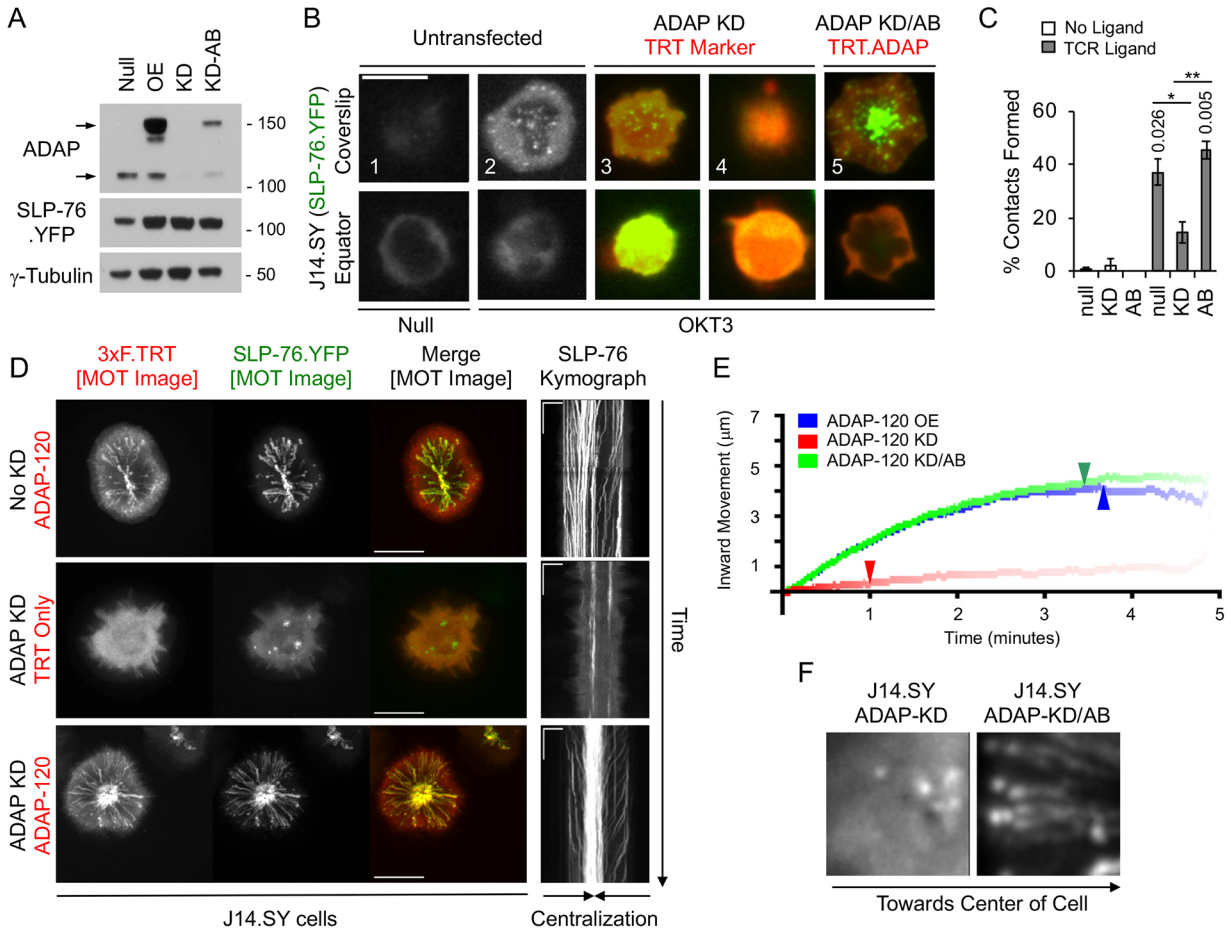

Fig. 2. ADAP enhances TCR-induced contact formation and microcluster dynamics. (A) J14.SY cells were transfected with vectors expressing 3×Flag.TRT.ADAP-120 (overexpression, OE), an ADAP-specific shRNA and 3×Flag.TRT (knockdown, KD), or an ADAP-specific shRNA and 3×Flag.TRT ADAP-120 (knockdown/addback, KD/AB). ADAP knockdown and re-expression were confirmed by western blotting. Results are representative of three experiments. Null, untransfected. Upper and lower arrows indicate the positions of the exogenous ADAP chimera and the endogenous ADAP protein, respectively. (B,C) Contact formation assays. J14.SY cells were used as untransfected controls or were transiently transfected with KD or KD/AB vectors, as above. Cells were injected into wells coated in the presence or absence of the stimulatory antibody OKT3. Cells were allowed to adhere for 10 min at 37°C, fixed, and imaged at or 5 µm above the plane of contact (coverslip or equator, respectively). (B) Selected images depicting spreading defects. SLP-76 is shown in grayscale or green; the markers for KD or KD/AB vectors are shown in red. Scale bar: 10 µm. Cell 1 failed to spread on a control substrate; cells 2, 3 and 5 spread on stimulatory substrates; cell 4 failed to spread on a stimulatory substrate. (C) Fractional adhesion was scored as in B for untransfected (null) J14.SY cells and TRT-positive KD and KD/AB cells (n=3 experiments, each scoring 3 fields in 2 wells per condition). All errors are displayed as s.e.m. *P<0.05; **P<0.01 compared with KD cells (Student's two-tailed t-test for unpaired samples). (D) J14.SY cells were transfected as above. OE, KD and KD/AB cells were stimulated, imaged and presented as in Fig. S2B (n=3 experiments; 30 TRT cells, 36 ADAP-KD cells, 30 ADAP-KD/AB cells). Scale bars: 10 µm (main images); 5 µm (horizontal); 60 s (vertical) (kymographs). (E) For the conditions in D, SLP-76 microcluster trajectories were manually traced in iVision and average trajectories are shown as composite kymographs. The x- and y-axes depict centripetal displacement over time and intensity encodes the fraction of clusters persisting; arrowheads indicate the time at which half of the microclusters had dissociated. Microcluster properties, number of cells analyzed, and statistical comparisons are listed in Table S2. (F) Regions of cells imaged in D are presented as 'standard deviation over time' images as in Fig. 1D. Sub-panels are 4.5 µm × 4.5 µm.

of endogenous ADAP (Fig. S3E; da Silva et al., 1997a; Raab et al., 1999).

Multivalent interactions hinder the de-phosphorylation of ADAP Y595

Although the Src-family kinase Fyn can bind ADAP via Y625, the Y625F mutation had no effect on the phosphorylation of Y595 (Fig. 4A) (da Silva et al., 1997a,b; Geng et al., 1999; Raab et al., 1999). In contrast, the mutation of the SLP-76-binding site at Y651 hindered the phosphorylation of Y595 following TCR stimulation. Given that an ADAP molecule can simultaneously interact with multiple SLP-76 SH2 domains, we postulated that Y651 phosphorylation could contribute to the stabilization of Y595 phosphorylation via the formation of a cooperatively stabilized oligomer capable of excluding tyrosine phosphatases. Consistent with this hypothesis, the Y651F mutation did not impact on the phosphorylation of Y595 in the presence of pervanadate, a broad-spectrum inhibitor of tyrosine phosphatases (Fig. 4B). Consistent with this model, overall tyrosine phosphorylation is greatly increased within the pool of ADAP that has been phosphorylated on Y595, relative to total ADAP (Fig. 4C), and Y595 phosphorylation was virtually eliminated when the SH2 domain of SLP-76 was inactivated (Fig. 4D). These findings indicate that even though TCR ligation induces extensive ADAP phosphorylation on sites other than Y595, very little of this tyrosine phosphorylation is preserved when either the

Journal of Cell Science (2018) 131, jcs215517. doi:10.1242/jcs.215517

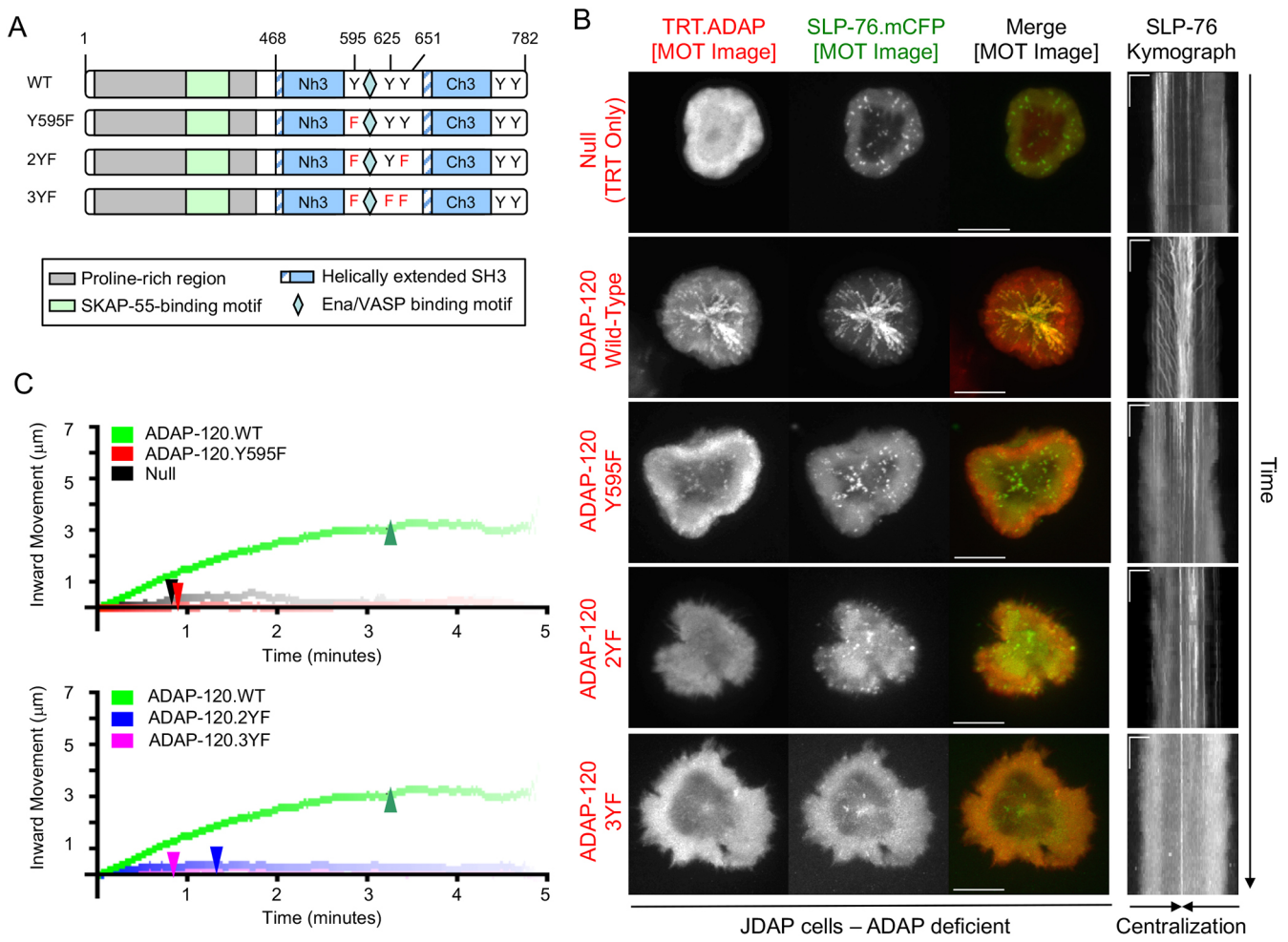

Fig. 3. Mutation of ADAP Y595 abolishes SLP-76 microcluster movement and persistence. (A) Schematic depiction of ADAP-120 chimeras with tyrosine to phenylalanine mutations at positions 595, 625 and 651. (B) ADAP-deficient (JDAP) cells transiently expressing the indicated 3×Flag.TRT-tagged chimeras and SLP-76.WT.mCFP were stimulated, imaged and presented as in Fig. 2 (*n*=3 experiments for all conditions except WT, which was *n*=4 experiments; see Table S3 for cell numbers). Scale bars: 10 µm (main images); 5 µm (horizontal); 60s (vertical) (kymographs). (C) For the conditions in B, SLP-76 microcluster trajectories were manually traced in iVision and average trajectories are shown as composite kymographs. The *x*- and *y*-axes depict centripetal displacement over time and intensity encodes the fraction of clusters persisting; arrowheads indicate the time at which half of the microclusters had dissociated. Microcluster properties, number of cells analyzed, and statistical comparisons are listed in Table S3.

SH2 domain of SLP-76 or its docking sites in ADAP are perturbed.

Individual mutations impacting on the SLP-76-binding Y651 or Y771 residues impair the phosphorylation of Y595 and antagonize microcluster stability

Using stably transduced J14.SY cells expressing near-endogenous levels of various ADAP chimeras, we tested the involvement of the SLP-76-binding tyrosine residues Y595, Y651 and Y771 in contact formation, Y595 phosphorylation, and the stabilization and movement of SLP-76 microclusters. In the context of low-level overexpression, chimeras with Y595F, Y651F, Y595F/Y651F (2YF) or Y771F mutations hindered the formation of TCR-induced contacts, as assessed by manual scoring (Fig. S4A). Although these mutants all impaired the TCR-induced phosphorylation of Y595, this loss was reversed by pervanadate treatment in the Y595-containing Y651F and Y771F single mutants (Fig. S4B). Imaging studies also revealed that the Y595F, Y651F, 2YF and Y771F mutants immobilized and/or destabilized SLP-76 microclusters (Fig. S4C–E). In contrast, the Y780F mutant, which affects a tyrosine residue that does not conform to the SLP-76 SH2 domain-binding motif, was statistically indistinguishable from WT ADAP in all respects. These data support the hypothesis that the multivalent interactions linking ADAP to SLP-76 contribute to the maintenance of ADAP phosphorylation (Fig. 4E).

The tyrosine-phosphorylated C-terminus of ADAP disrupts SLP-76 microclusters

To clarify how ADAP participates in SLP-76 microclusters, we deleted the N-terminus of ADAP (Fig. 5A). The resulting C-terminal fragment of ADAP-120, which contains all known SLP-76 SH2 domain-binding sites, failed to associate with the plasma membrane in J14.SY cells. Although this fragment was inducibly phosphorylated at the SLP-76 SH2 domain-interacting Y595 site, the stoichiometry of phosphorylation was much lower than for endogenous ADAP, indicating that the N-terminus normally facilitates ADAP phosphorylation (Fig. S5). In contrast to WT ADAP-120, the C-terminal fragment was not observed in SLP-76 microclusters, demonstrating that the N-terminus also stabilizes ADAP within microclusters (Fig. 5B). Furthermore, the C-terminal fragment of ADAP potently inhibited microcluster persistence and movement even though the phosphorylation of endogenous ADAP

Journal of Cell Science (2018) 131, jcs215517. doi:10.1242/jcs.215517

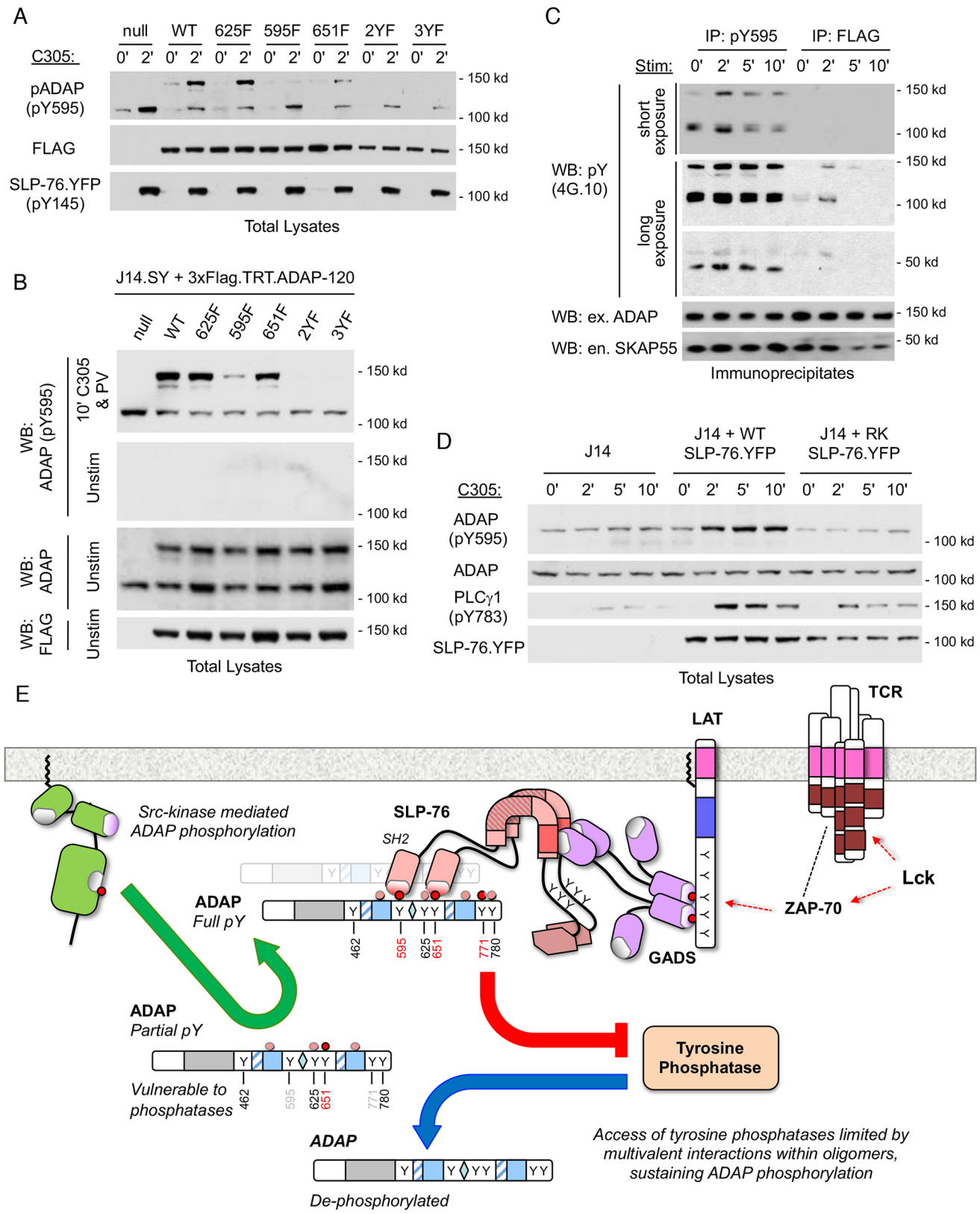

Fig. 4. See next page for legend.

was unimpaired (Fig. 5B,C; Table S2, Movie 12, Fig. S5). In contrast, C-terminal fragments with the Y595F, 2YF and 3YF mutations (Fig. 5A) were not phosphorylated on Y595 (Fig. S5B) and were less capable of antagonizing microcluster formation (Fig. 5B,C; Table S2, Movie 13). To explain these phenomena, we postulate that the phosphorylated C-terminal fragment of ADAP is capable of forming stable oligomers with LAT, Gads and SLP-76, but is unable to integrate these oligomers into persistent

Journal of Cell Science (2018) 131, jcs215517. doi:10.1242/jcs.215517

Fig. 4. Multivalent interactions of ADAP with SLP-76 stabilize ADAP phosphorylation. (A) J14.SY cells were stably transduced with lentiviruses encoding the indicated 3×Flag.TRT.ADAP-120 chimeras. Parental and transduced cells were either left unstimulated or stimulated with C305 for 2 min. Total lysates were western blotted (WB) as indicated. FLAG serves as a loading control while pY145 SLP-76 indicates TCR activation. (B) J14.SY cells stably expressing the indicated ADAP chimeras were left unstimulated or stimulated with pervanadate and C305 for 10 min. Total lysates were western blotted for FLAG, total ADAP or ADAP pY595. (C) J14.SY cells stably expressing 3×FLAG.TRT.ADAP were stimulated with C305 and lysed. Y595-phosphorylated ADAP (pY595) and total ADAP (FLAG) were immunoprecipitated (IP) using fixed amounts of each antibody and oversaturating amounts of lysate. This ensured that the total amount of ADAP captured by the pY595 antibody was fixed, regardless of the time of stimulation. Each FLAG IP contained 30 times more total ADAP than the corresponding pY595 IP. Equal amounts of total ADAP were loaded and western blotted for ADAP, SKAP55, and total phosphotyrosine (pY). ex., exogenous; en., endogenous. (D) Parental J14 cells or J14 cells stably reconstituted with WT (WT) or SH2 mutant (RK) SLP-76.YFP chimeras were stimulated, lysed and western blotted for ADAP pY595. pY783 PLCγ1 serves as a control for TCR signaling. All western blots are representative of three or more independent experiments. (A–D) For all western blots, the SLP-76.YFP chimera migrates just above the 100 kDa marker, endogenous ADAP migrates just above the SLP-76 chimera and 3xFlag-TRT-tagged ADAP chimeras migrate just below 150 kDa; endogenous SKAP55 migrates just below 50 kDa. Time of stimulation is given in minutes. (E) Model for the SLP-76 SH2 domain-dependent maintenance of ADAP phosphorylation: TCR ligation results in the Lck-dependent activation of ZAP-70, triggering the formation of oligomers containing LAT, Gads and SLP-76 (top right). Concurrently, small populations of ADAP become phosphorylated by a Src kinase (green arrow). Heavily phosphorylated ADAP species capture LAT–SLP-76 oligomers via multivalent interactions between the SLP-76 SH2 domain and tyrosine residues 595, 651 and 771 of ADAP (red circles), shielding ADAP from dephosphorylation (red blocking arrow). In contrast, partially phosphorylated ADAP is de-phosphorylated by cytoplasmic phosphatases (blue arrow). The sites of other tyrosine-phosphorylated residues in ADAP are based on mass spectroscopy studies (pale circles) (Lange et al., 2010; Sylvester et al., 2010).

microclusters. In contrast, the non-phosphorylatable variants cannot compete with endogenous ADAP for access to nascent LAT–Gads–SLP-76 oligomers.

Tyrosine phosphorylation at Y595 distinguishes two pools of ADAP

We observed that ADAP is typically enriched in the actin-rich structures that surround the contact, and that the fraction of ADAP in these structures is often inversely correlated with the recruitment of ADAP into microclusters (Fig. S2B; Fig. 2D; Fig. 3B). Since the phosphorylation of Y595 was required for the entry of ADAP into SLP-76 microclusters, we postulated that the lamellipodial pool of ADAP was not phosphorylated at this site. To test this hypothesis, we took advantage of the flow-through of the antiserum from which our pY595-specific reagent was developed. After serial depletion on the immunizing phosphopeptide, this serum was affinity purified on the un-phosphorylated peptide, giving rise to a reagent that recognizes both endogenous and exogenous ADAP in unstimulated cells, but that displays reduced reactivity towards the extensively phosphorylated ADAP species observed after TCR stimulation and pervanadate treatment (Fig. 6A). In J14.SY cells stably expressing exogenous ADAP at near-physiological levels, Y595-phosphorylated ADAP was restricted to SLP-76-positive microclusters and to small peripheral speckles that lack SLP-76, while non-phosphorylated ADAP was found at the boundary of the contact and was most enriched at the outermost edge of this region (Fig. 6B). Similar patterns were observed in J14.SY cells lacking exogenous ADAP, confirming that these distributions are not artifacts of our tagging strategy (Fig. 6C). To confirm whether the peripheral ADAP structures were adherent, we sheared away the responding T cells, leaving behind only the adhesive structures that were tightly coupled to the stimulatory substrate (Ophir et al., 2013). After shearing, ADAP was retained in SLP-76 microclusters, but no ADAP was observed outside of these structures (Fig. 6D, upper panels). Furthermore, the pY595-phosphorylated pool of ADAP was also retained in TCR-adherent SLP-76 microclusters (Fig. 6D, lower panels). We conclude that most of the ADAP in the actin-rich boundary of the contact is found within cytoskeletal structures that have not yet initiated adhesive contacts and can be stripped away, whereas the clustered, Y595-phosphorylated pool of ADAP is firmly attached to the substrate. This population of ADAP may contribute to TCR-mediated adhesion and to the stabilization of the contact boundary. Importantly, these data indicate that Y595 phosphorylation mediates the re-distribution of ADAP from peripheral protrusive structures to the integrin-independent adherent junctions associated with SLP-76 microclusters.

Non-phosphorylated ADAP is enriched in peripheral actin-rich structures

To confirm that ADAP associates with lamellipodial actin, we transfected J14.SY cells with 3×Flag.TRT.ADAP-120 and either monomeric CFP (mCFP) or an mCFP-tagged form of β-actin. As expected, ADAP entered two distinct pools: a peripheral pool coincident with lamellipodial actin and a clustered pool coincident with SLP-76 (Fig. 7A, left panels). To illustrate the degree of colocalization between ADAP and actin, we pre-processed the images in order to remove any regions containing SLP-76 microclusters, and then determined the relative enrichments of ADAP, β-actin and the mCFP control relative to the cytoplasmic pool of SLP-76 (Fig. 7A, right panels; see Materials and Methods). By using this method, we confirmed that the ratio of mCFP to SLP-76 was uniform throughout the cell, verifying this approach. In contrast, the ratios of ADAP and β-actin to cytoplasmic SLP-76 revealed dramatic enrichments in the periphery of the contact, confirming the association of ADAP with peripheral actin-rich structures.

Actin-rich structures ‘pre-position’ ADAP at sites of contact and microcluster nucleation

The tips of actin-rich protrusions are enriched in proteins that facilitate Arp2/3-dependent actin polymerization, including WASP, WAVE and Ena/VASP family proteins (Krause et al., 2000; Zipfel et al., 2006). The tips of these structures also give rise to stimulatory junctions during contact initiation and expansion (Bunnell et al., 2001; Seminario and Bunnell, 2008; Bunnell, 2010; Cai et al., 2017). As ADAP interacts with several of these tip-associated proteins, we reasoned that the association of ADAP with these structures could pre-position ADAP at future sites of TCR engagement and microcluster nucleation, thereby enabling ADAP to interact with and stabilize nascent LAT–SLP-76 complexes (Krause et al., 2000; Pauker et al., 2011, 2014). Consistent with this hypothesis, ADAP was enriched in puncta and sheet-like projections that reached down from the cell body towards the stimulatory surface (Fig. 7B; Movie 14). Analogous triple-color studies including mCFP.β-actin confirmed that these structures contain actin and are likely to be filopodial and/or lamellipodial protrusions (Fig. S6). As contacts mature, these actin- and ADAP-containing structures expanded and dissociated, while new structures continued to form underneath landing cells and at the boundaries of expanding contacts. Discrete points within these

Journal of Cell Science (2018) 131, jcs215517. doi:10.1242/jcs.215517

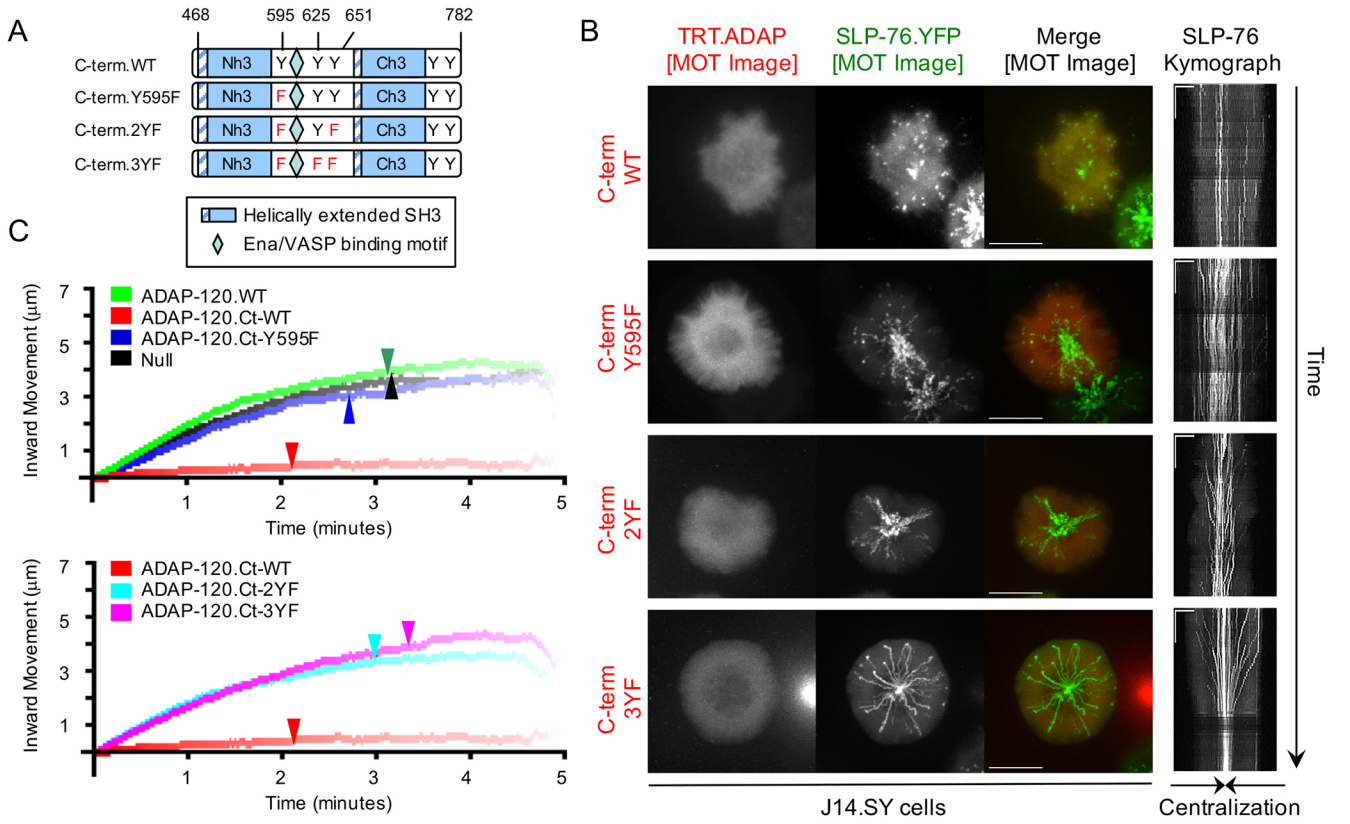

Fig. 5. The C-terminus of ADAP destabilizes SLP-76 microclusters in a phosphotyrosine-dependent manner. (A) Schematic of 3×FLAG.TRT-tagged ADAP C-terminal chimeras with phenylalanine mutations at specific tyrosine residues. (B) J14.SY cells transiently expressing the indicated 3×FLAG.TRT-tagged chimeras were stimulated, imaged, and presented as in Fig. 2. ADAP-120 C-term.WT (n=5 experiments), C-term mutants (n=3 experiments each), see Table S2 for cell numbers and microcluster properties. Scale bars: 10 µm (main images); 5 µm (horizontal); 60 s (vertical) (kymographs). (C) For the conditions in B, SLP-76 microcluster trajectories were manually traced in iVision and average trajectories are shown as composite kymographs. The x- and y-axes depict centripetal displacement over time and intensity encodes the fraction of clusters persisting; arrowheads indicate the time at which half of the microclusters had dissociated.

structures gave rise to SLP-76 microclusters, and ADAP persisted at these sites, even after actin had cleared away (see the rightmost panel of Fig. S6).

Although SLP-76 contributes to the development of the immune synapse, the SLP-76 SH2 domain is dispensable for the transient enrichment of ADAP in contact structures

In control J14 cells expressing ADAP and mYFP, sheet-like lamellipodial structures were virtually absent, while ADAP remained largely cytoplasmic (Movie 15). Nevertheless, small protrusions formed and were resorbed at the boundary of the contact. J14 cells co-expressing ADAP and WT SLP-76 formed stable synapses surrounded by small, discontinuous peripheral lamellipodia; in these cells SLP-76 and ADAP were preferentially co-enriched in microclusters (Fig. 7C,D, upper panels; Movie 16). In contrast, in J14 cells co-expressing ADAP with the SH2 domain-inactivated form of SLP-76, ADAP entered the large dynamic lamellipodia that surrounded the contact and was largely absent from the labile SLP-76 microclusters that formed under these conditions (Fig. 7C,D, lower panels; Movie 17). Nevertheless, ADAP was transiently enriched at the sites that subsequently gave rise to short-lived SLP-76 microclusters (Fig. 7D, red arrows). Thus, ADAP is transiently recruited to nascent signaling complexes despite its inability to interact with the SLP-76 SH2 domain. These findings support a model in which ADAP is pre-positioned at potential TCR contact sites via its interactions with protrusive actin structures, becomes locally phosphorylated in response to TCR engagement, engages the SH2 domain of SLP-76, is protected from dephosphorylation via the formation of a multivalent oligomer, and contributes to the consolidation of these structures into SLP-76 microclusters via interactions involving its N-terminal domain (Fig. 8). Finally, these findings indicate that ADAP is not simply a downstream effector that is recruited to SLP-76 but is instead a co-equal participant in the assembly of persistent and mobile SLP-76 microclusters.

DISCUSSION

Here, we demonstrate that the interaction between ADAP and SLP-76 promotes the mutual retention of both adaptors within TCR-induced microclusters and enables the cohesion, persistence and sustained movement of these signaling complexes. This interaction also supports the attachment of T cells to anti-CD3ε-coated glass substrates in the absence of integrin–ligand interactions. By using a novel phospho-specific antibody, we demonstrate that the Y595-phosphorylated pool of ADAP is further phosphorylated in response to TCR ligation and postulate that ADAP phosphorylation is facilitated by the N-terminal domain responsible for cytoskeletal association and is stabilized through the formation of multivalent complexes that hinder the tonic de-phosphorylation of ADAP. The phosphorylation of ADAP on Y595 is also associated with the movement of ADAP from a peripheral, actin-associated pool into SLP-76 microclusters. Finally, cytoskeletal structures deliver non-phosphorylated ADAP to sites of potential TCR engagement, without regard for the capacity of ADAP to engage SLP-76. In light of these

Journal of Cell Science (2018) 131, jcs215517. doi:10.1242/jcs.215517

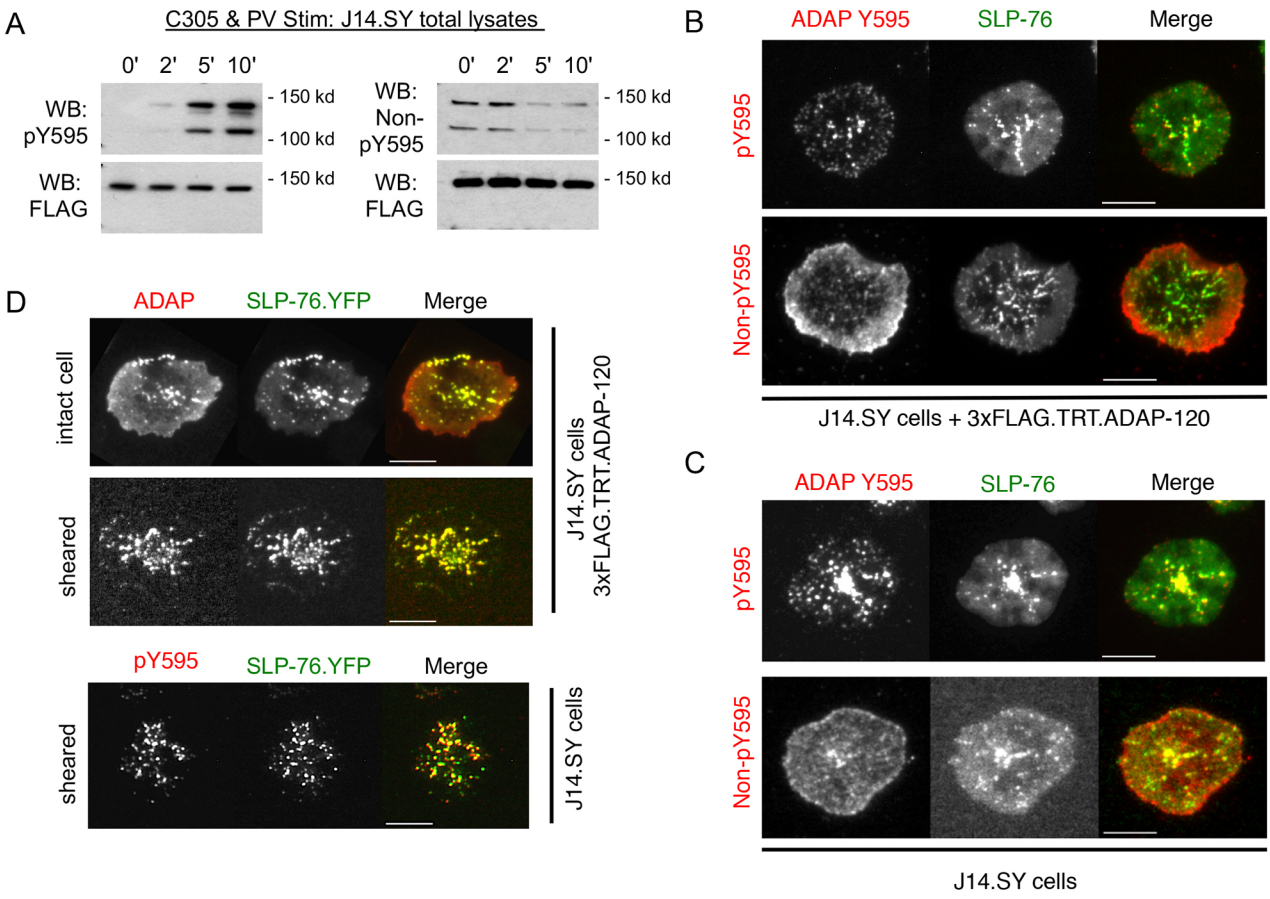

Fig. 6. Tyrosine phosphorylation controls the localization of ADAP between the actin-rich leading edge and SLP-76 microclusters. (A) J14.SY cells stably expressing 3×Flag.TRT.ADAP-120 were co-stimulated with C305 and pervanadate for the indicated times. Total lysates were western blotted (WB) with custom antisera specific for phosphorylated or non-phosphorylated Y595 (pY595 and non-pY595, respectively) or with an anti-FLAG control antibody. The dominant bands are exogenous (upper) and endogenous (lower) ADAP. The image shown is representative of three independent experiments. (B) J14.SY cells stably expressing exogenous 3×Flag.TRT.ADAP-120 were stimulated as in Fig. 1 and fixed after 10 min. Fixed cells were stained with ADAP antisera targeting phosphorylated pY595 (*n*=3 experiments, 33 cells) or non-pY595 (*n*=3 experiments, 42 cells). (C) J14.SY cells without exogenous ADAP expression were stimulated as in Fig. 1 and fixed after 10 min. Fixed cells were stained with ADAP antisera targeting pY595 (*n*=3 experiments, 65 cells) or non-pY595 (*n*=3 experiments, 34 cells). (D) J14.SY cells stably expressing 3×Flag.TRT.ADAP-120 were stimulated as in Fig. 2 and fixed. Before imaging, cell bodies were left intact (upper row) or sheared away, leaving only the cell footprint (middle row). In the bottom row, J14.SY cells without exogenous ADAP expression were sheared away from the substrate prior to immunofluorescence staining of the residual adherent structures with pY595 sera (*n*=2 experiments; 31 WT unsheared cells, 54 WT sheared cells, 19 J14.SY sheared cells). Scale bars: 10 µm.

findings, we favor a revised model of T cell activation in which the TCR is coupled to SLP-76 via two cooperative pathways: one that involves the canonical LAT–Gads complex originating in lipid rafts, and a second that involves pre-positioned ADAP molecules capable of retaining SLP-76 oligomers at sites of TCR engagement and microcluster assembly (Fig. 8). The latter pathway may explain the observation that SLP-76 phosphorylation is not reduced in Gads-deficient Jurkat cells (Lugassy et al., 2015).

Although this study is largely consistent with previous work, it provides new insights into the dynamics of microcluster formation (Baker et al., 2009; Pauker et al., 2011; Coussens et al., 2013). Specifically, the inactivation of the SLP-76 SH2 domain or the elimination of ADAP immobilizes and destabilizes SLP-76 microclusters, without precluding their formation. Furthermore, these perturbations fundamentally alter the behavior of SLP-76 microclusters, such that the *en bloc* centripetal movement of the cluster is abolished, while SLP-76 microclusters continuously shed smaller particles that depart rapidly, in all directions. These manipulations also produce changes in contact morphology consistent with previous reports, while also yielding changes in the frequency of contact formation, the stability of the contact boundary, the adhesion of T cells to stimulatory substrates and the induction of CD69 expression. While most perturbations that destabilize SLP-76 microclusters impair the production of second messengers, we observe no impacts on TCR-induced PLCγ1 phosphorylation, ERK1/2 phosphorylation or Ca^{2+} entry (Singer et al., 2004; Bunnell et al., 2006; Houtman et al., 2006; Sylvain et al., 2011). Although our findings regarding Ca^{2+} entry conflict with a recent report by Coussens et al., earlier studies in murine models confirm that the SLP-76 SH2 domain is dispensable for TCR-initiated Ca^{2+} and ERK1/2 responses (Griffiths et al., 2001; Myung et al., 2001; Peterson et al., 2001; Burns et al., 2011; Coussens et al., 2013). We postulate that the work by Coussens et al. may have captured a subtle defect in Ca^{2+} entry by using a lower dose of stimulatory antibody (6.25 ng/ml) than the current work (30 ng/ml).

Residues Y595 and Y651 of ADAP are well-established SLP-76 SH2 domain-binding sites that contribute to the biological functions of ADAP (Geng et al., 1999; Raab et al., 1999; Wang et al., 2004, 2009; Lange et al., 2010; Pauker et al., 2011; Coussens et al., 2013).

Journal of Cell Science (2018) 131, jcs215517. doi:10.1242/jcs.215517

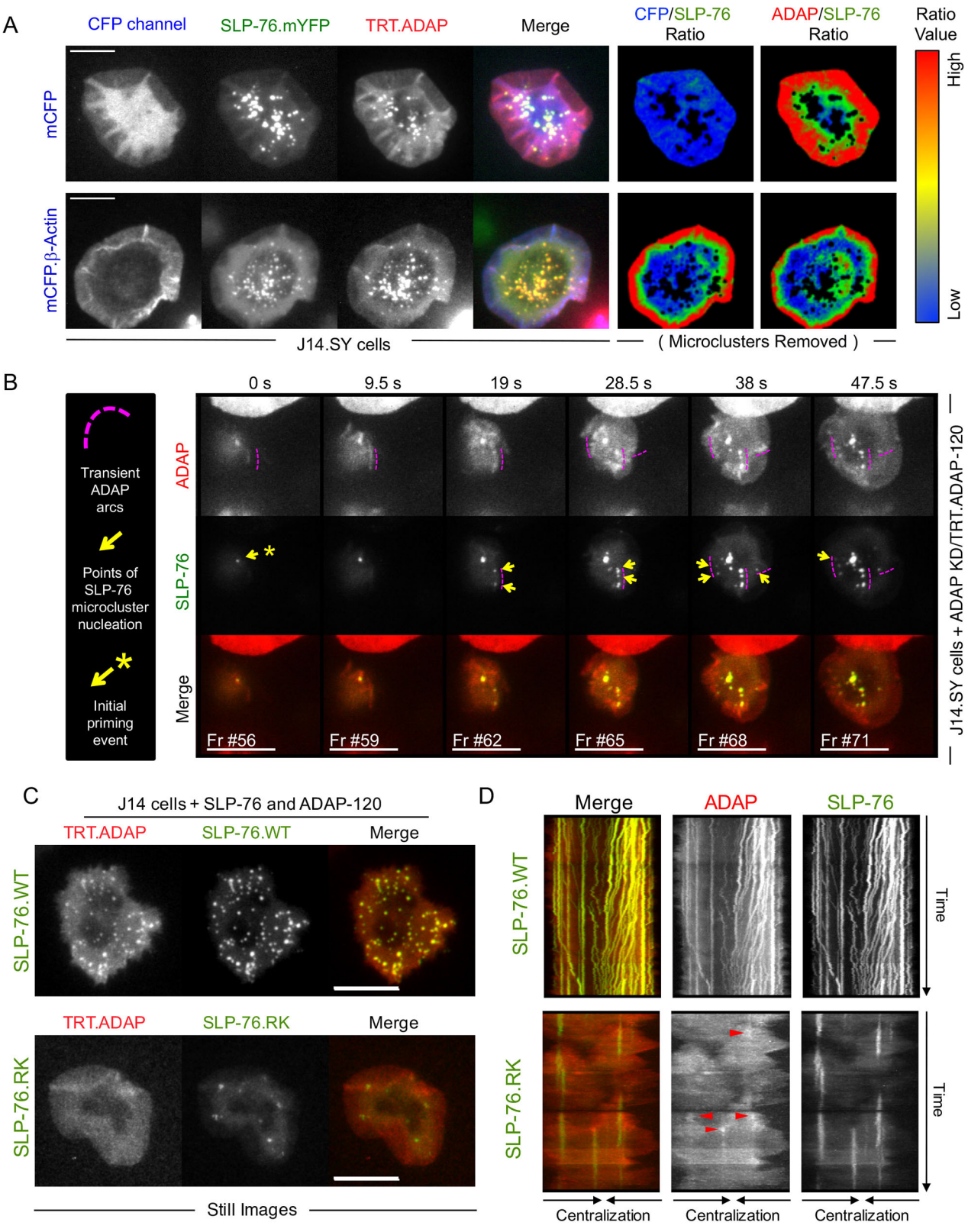

Fig. 7. See next page for legend.

A third tyrosine, Y771, is a lower affinity binding site for SLP-76 and has also been implicated in transmission of signals downstream of the TCR. In contrast to previous studies, which have examined the behavior of ADAP mutants in the context of WT ADAP, we show that Y595 is strictly required for the persistence and movement of SLP-76 microclusters when endogenous ADAP is absent. Using our novel phospho-specific antiserum, we provide the first direct evidence for the phosphorylation of Y595 in TCR-stimulated

Journal of Cell Science

Journal of Cell Science (2018) 131, jcs215517. doi:10.1242/jcs.215517

Fig. 7. ADAP enters actin-rich junctional structures prior to and independently of SLP-76. (A) J14.SY cells transiently expressing 3×Flag.TRT.ADAP-120 and either CFP or CFP.β-actin were stimulated and imaged as described in Fig. 2. Left, representative still panels showing examples of the variable enrichment of ADAP in actin and in SLP-76 microclusters (*n*=2 experiments; mCFP, 4 cells; CFP.β-actin, 16 cells). Right, edge enrichment of ADAP relative to cytoplasmic SLP-76. Masking operations were performed to remove regions with SLP-76 microclusters. Ratiometric images are shown, using the scale on the right, for mCFP, CFP.β-actin and TRT.ADAP normalized to SLP-76. (B) Representative images depicting the first moments of cellular contact. Dashed arcs identify three different ADAP-rich protrusive structures contacting the substrate. Yellow arrows emphasize SLP-76 microcluster formation along these ADAP arcs, with the yellow asterisk indicating the first microcluster nucleation event (*n*=3 experiments, 7 cells captured during contact formation). Fr #, frame number. (C) J14 cells transiently expressing 3×Flag.TRT.ADAP-120 and the indicated YFP chimeras were stimulated and imaged as in Fig. 1. Still images are shown. (D) Representative kymographs derived from J14 cells stimulated and imaged after transient expression of TRT.ADAP-120 and SLP-76.WT.mYFP (top) or SLP-76.RK.mYFP chimeras (bottom). Red arrows indicate sites of transient co-clustering of SLP-76 and ADAP in J14 cells expressing the SLP-76.RK mutant (*n*=2 experiments, 11 ADAP/WT cells, 4 ADAP/RK cells). Scale bars: 10 µm (main images); kymographs in D are 18 µm (horizontal) by 6.5 min (vertical).

T cells, show that Y595 phosphorylation requires Src kinase activity, and reveal that the TCR-induced tyrosine phosphorylation of ADAP on all other sites is restricted to molecules phosphorylated on Y595. Furthermore, we provide evidence that the physiological phosphorylation of ADAP is dependent on the formation of a multivalent complex involving Y595, Y651, Y771 and the SH2 domain of SLP-76. Finally, we show that the phosphorylation of ADAP Y595 loses its dependence on Y651 and Y771 in the presence of the tyrosine phosphatase inhibitor, pervanadate. Since ADAP interacts with immunologically relevant tyrosine phosphatases, including TCPTP (*PTPN2*), SHP1 (*PTPN6*) and SHP2 (*PTPN11*), the acute phosphorylation of ADAP may require the competitive exclusion of tyrosine phosphatases by multivalent scaffolding interactions and/or the inhibition of tyrosine phosphatases by microcluster-associated effectors (Fig. 4E) (Kwon et al., 2005; Lehmann et al., 2009; Lange et al., 2010; Wiede et al., 2011; Coussens et al., 2013).

Using these tools, we have also shown that non-phosphorylated ADAP is enriched at the tips of actin-rich protrusions, and only enters SLP-76 microclusters following its phosphorylation on Y595. Since these cytoskeletal structures generate the tight contacts that enable TCR engagement (Bunnell et al., 2001, 2002; Cai et al., 2017), the pre-positioning of ADAP at these sites may ensure that ADAP is available to trap nascent SLP-76 oligomers and assemble them into microclusters. Consistent with this hypothesis, the deletion of the N-terminus, which eliminates ADAP from these actin-rich sites, causes the residual C-terminal fragment of ADAP to antagonize microcluster stability and movement. Although SKAP55 is the best-characterized binding partner of the ADAP N-terminus, it remains cytoplasmic in the absence of ADAP. Therefore, distinct ADAP-interacting proteins may mediate the recruitment of ADAP into protrusive cytoskeletal structures (Yuan et al., 2005; Ophir et al., 2013; Kasirer-Friede et al., 2014).

The subdivision of ADAP into pools differentiated by phosphorylation states is remarkably reminiscent of the work by Burbach et al., who reported that distinct pools of ADAP are involved in the regulation of integrin activation and the activation of NF-κB. In these studies, SKAP55, and, in particular, the lipid-binding pocket of the SKAP55 pleckstrin homology domain, played a decisive role in the ability of ADAP to participate in the regulation of integrins as opposed to the activation of NF-κB (Burbach et al., 2008, 2011). Since our studies were conducted in Jurkat cells, which display constitutively high levels of phosphatidylinositol (3,4,5)-

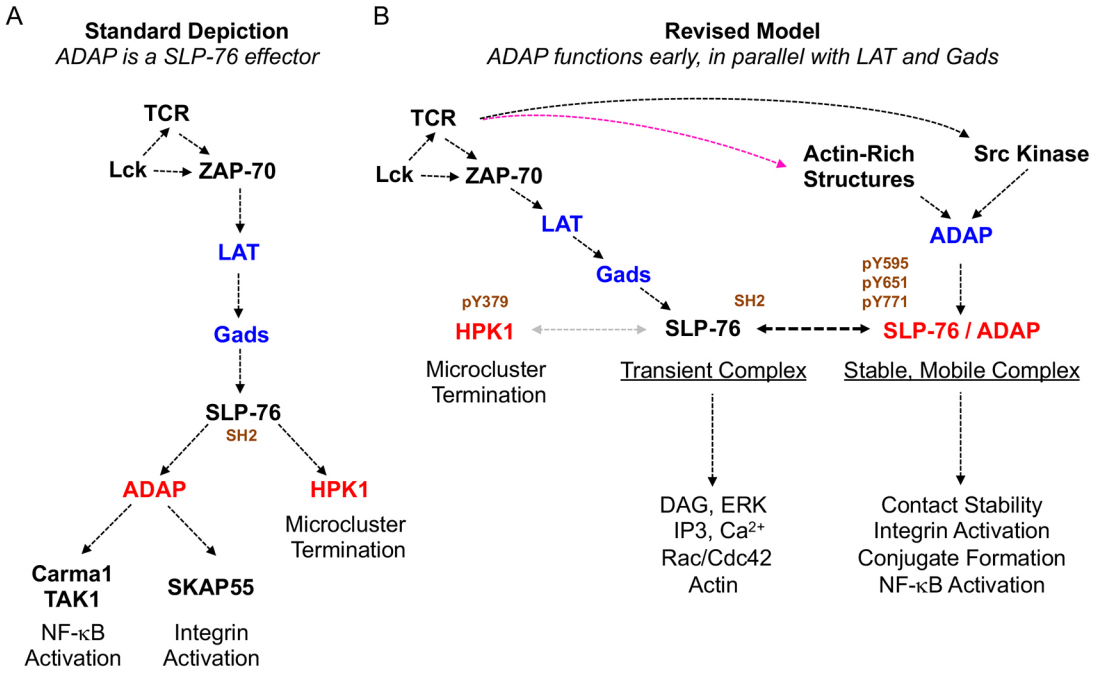

Fig. 8. ADAP provides a parallel mechanism of SLP-76 recruitment by immunoreceptors and is an integral component of cohesive SLP-76 microclusters. (A) ADAP is conventionally depicted as playing the role of a terminal effector downstream of SLP-76 to mediate NF-κB and integrin activation. (B) We propose an alternative model in which SLP-76 and ADAP function in parallel pathways downstream of the TCR and intersect at the level of the SLP-76 microcluster to allow for complex stability and productive signaling.

Journal of Cell Science (2018) 131, jcs215517. doi:10.1242/jcs.215517

trisphosphate, it is likely that the observations presented here are biased towards the role of ADAP in integrin activation (Shan et al., 2000). Therefore, although further studies will be required to clarify the parallels between these systems, we postulate that the Y595-phosphorylated pool of ADAP is crucial for integrin activation but is less important for the activation of NFκB (Ophir et al., 2013).

Normal SLP-76 microclusters form at discrete foci in the periphery of the contact and depart their sites of nucleation, either *en bloc* or by fission from a pool of SLP-76 that is retained at the nucleation site. After departing these sites, SLP-76 microclusters undergo directed centripetal movement. In contrast, the disruption of the interaction between SLP-76 and ADAP results in labile microclusters that are less sharply defined and display unusually dynamic changes in morphology. For instance, these altered clusters continuously shed SLP-76 via small, fast moving particles that do not exhibit directional movements. We suggest that this represents a defect in microcluster cohesion and results from the failure of nascent microclusters to resist endocytic termination. Several mechanisms may contribute to this phenotype. First, the interaction between SLP-76 and ADAP may simply enhance the overall avidity of the interactions that maintain SLP-76 microclusters. Second, in the absence of ADAP, the serine-threonine kinase HPK1 may gain increased access to microclusters, which it may destabilize by promoting the ubiquitylation and degradation of SLP-76 and Gads (di Bartolo et al., 2007; Shui et al., 2007; Patzak et al., 2010; Lasserre et al., 2011; Wang et al., 2012; Coussens et al., 2013). Third, ADAP may contribute to the exclusion or inactivation of the Cbl family E3 ubiquitin ligases, which promote the degradation of LAT, SLP-76, Vav1 and WASP, and attenuate microcluster lifetimes (Krawczyk et al., 2000; Miura-Shimura et al., 2003; Chiang et al., 2004; Barr et al., 2006; Balagopalan et al., 2007, 2011; Chiang et al., 2009; Chiang and Hodes, 2011; Reicher et al., 2012). Finally, the cohesion defect observed in the absence of ADAP may stem from the dysregulation of the bounding 'micro-adhesion rings' recently described by Hashimoto-Tane et al. (Hashimoto-Tane et al., 2016). These integrin-associated rings contribute to the retention of LAT and SLP-76 within microclusters, and, like ADAP, are important for the responses of T cells to low doses of antigens (Mueller et al., 2007). Since super-resolution imaging studies have shown that SLP-76 is enriched at the outer margin of the microcluster, ADAP could function as a bridge between the microcluster and the surrounding micro-adhesion rings by linking SLP-76 to integrin-associated cytoskeletal proteins such as RapL, RIAM, talin and kindlin-3 (Menasche et al., 2007; Raab et al., 2010; Sherman et al., 2011, 2016; Kliche et al., 2012; Ophir et al., 2013; Kasirer-Friede et al., 2014).

In conclusion, ADAP plays crucial roles in the cohesion and sustained movement of SLP-76 microclusters. Like SKAP55, ADAP endows SLP-76 microclusters with integrin ligand-independent adhesive functions and contributes to the stability of the interfaces that link T cells to stimulatory substrates (Ophir et al., 2013). These functions require the protection of ADAP from de-phosphorylation by the multivalent network of interactions that links ADAP to SLP-76. In addition, these functions require the presence of the N-terminus of ADAP, which links ADAP to the protrusive cytoskeletal systems that enable ligand recognition by the TCR. Through its interactions with cytoskeletal structures, ADAP arrives at nascent contacts in advance of SLP-76, where it enables the recruitment of SLP-76 into persistent microclusters. Overall, our studies indicate that the signaling hierarchy downstream of the TCR should be revised to place LAT and ADAP in parallel pathways that cooperate to generate persistent SLP-76 microclusters and TCR-dependent adhesive junctions (Fig. 8).

MATERIALS AND METHODS

Plasmid constructs

Fluorescent protein tagging vectors based on pEGFP-c1 and pEGFP-n1 (Clontech, Mountain View, CA), but encoding conventional and monomeric forms of YFP and CFP have been described (Zacharias et al., 2002). Tagging vectors encoding TagRFP-Turbo (TRT) were generated by PCR from templates provided by Roger Tsien (Dept. of Chemistry and Biochemistry, University of California San Diego, CA) (Shaner et al., 2008). Where indicated, sequences encoding triple FLAG epitope tags (3×Flag) were appended 5′ to the fluorescent protein. The vector expressing HA-tagged *Homo sapiens* SLP-76.YFP has been described previously (Bunnell et al., 2002). The SLP-76 R448K mutation (SLP-76.RK) was introduced by overlap extension PCR. Inserts encoding WT and R448K mutant forms of *Mus musculus* SLP-76 were recovered from vectors encoding EGFP.mmSLP-76 chimeras by PCR and were subcloned into the same framework as human SLP-76 (Bunnell et al., 2006; Singer et al., 2004). The cDNAs for *H. sapiens* ADAP-120 and ADAP-130 were recovered from total Jurkat cDNA (SMART cDNA Synthesis Kit, Clontech) by PCR and subcloned into fluorescent protein-tagging vectors. ADAP expression was driven by either the SRα promoter or a modified EF1α promoter. SLP-76 chimeras are 2×HA.L1.SLP-76.L2.YFP and ADAP chimeras are 3×Flag.L3.TRT.L4.ADAP, with all components labeled from the N-terminus to the C-terminus, and where L1-L4 refer to linker sequences. All proteins retain their initial methionine residues. The amino acid sequences of the tags and linkers are as follows: 2×HA, MIFYPYDVPDYAGYPYDVPDYAG; 3×Flag, MYDYKDDDDKDYK DDDDKDYKDDDDK; L1, STSRSPGRAA; L2, GGGAGARDPPVAT; L3, PMTPVAT; and L4, SGLRSRDAT. The ADAP-specific short hairpin RNA (shRNA) targets a sequence present in the 3′ untranslated region, 5′-GTATGCACATTGAAGTCTA-3′, and was constructed in the suppression vector pFRT-H1/Hygro, provided by Daniel Billadeau (Dept. of Immunology, Mayo Clinic, MN). The resulting H1-driven shRNA cassette was PCR amplified and subcloned into SRα-driven vectors expressing either 3×Flag.TRT or 3×Flag.TRT.ADAP-120, placing the shRNA cassette upstream of the SRα promoter. All ADAP chimeras lack the native 3′ UTR and are hairpin-resistant. ADAP tyrosine mutants and C-terminal fragments were generated by overlap extension PCR and subcloned into Clontech c1-type vectors. To facilitate the production of stable cell lines the 2×HA.hsSLP-76.YFP chimeras were subcloned into lentiviral expression vectors based on pLEX-MCS (Open Biosystems, Grand Island, NY), while the ADAP chimeras were subcloned into related vectors lacking the IRES-puromycin cassette. The lentiviral packaging vector psPAX2 (plasmid 12260; Addgene, Cambridge, MA,) and the VSV-G pseudotyping vector pMD2.G (plasmid 12259; Addgene) were developed by Didier Trono.

Cell lines and transfections

The SLP-76-deficient (J14) Jurkat T cell line and the SLP-76-deficient Jurkat T cell line reconstituted with YFP-tagged SLP-76 (J14.SY) were described previously (Bunnell et al., 2006). The ADAP-deficient (JDAP) Jurkat T cell line was supplied by Ron Wange (Huang et al., 2005). Transfections were described previously (Bunnell et al., 2006). J14.SY cells stably expressing WT and mutant ADAP chimeras were generated by lentiviral infection and flow cytometry-based sorting for matched levels of SLP-76.mYFP and TRT.ADAP. Jurkat T cell culture was previously described (Huang et al., 2005; Bunnell et al., 2006). Cell lines were validated by verifying that the parental lines were only deficient in the relevant molecules when western blotted for other proteins involved in the TCR signaling pathway, including ZAP-70, LAT, PLCγ1, SLP-76, ADAP and Lck. The 293T human renal epithelial cells were cultured in Dulbecco's modified Eagle's medium (DMEM, Cellgro, Tewksbury, MA) supplemented with 10% fetal calf

serum, 2 mM L-glutamine, 100 units/ml penicillin and 100 µg/ml streptomycin, in a humidified incubator with 5% CO_2.

Lentiviral production and infection

Packaging reactions used 293T cells at ∼70% confluency. For each 10 cm plate, a mix of 18 µl FuGENE 6 Transfection Reagent (Roche, Mannheim, Germany) and 142 µl serum-free DMEM was prepared and incubated at room temperature for 5 min. In parallel, lentiviral vectors (3 µg pLEX-based plasmids) were combined with 1.5 µg psPAX2 packaging plasmid and 0.5 µg pMD2.G envelope plasmid in 40 µl of serum-free DMEM. The cocktails were combined and incubated at room temperature for 30 min. The DNA/FuGENE cocktail was added to 293T cells and after 12–15 h, the transfection mixture was replaced with fresh DMEM. Lentiviral supernatants were harvested 66–72 h post transfection. To transduce Jurkat cells, equal parts of fresh RPMI, Jurkat cells, and lentiviral supernatants were combined. Infection rates were assessed after 48 h and exceeded 50%.

Antibodies

T cells were stimulated with antibodies specific for CD3ε (OKT3, 10 µg/ml per well, BioExpress Cell Culture Services, Radnor, PA) or the Vβ8 subunit of the TCR (C305, 1:500, from Gary Koretzky, Weill Cornell Medical College, New York, NY, USA). Rabbit antibodies targeting the Y595 phosphorylated and Y595 non-phosphorylated forms of ADAP were developed at Pacific Immunology (Ramona, CA) using the synthetic immunogen EDDQEVpYDDVAEQD. The phospho-specific 'pY595' antibody was obtained by affinity purification on the immunizing phosphopeptide and depletion against the non-phosphorylated peptide. Conversely, the flow-through remaining after the initial purification step was affinity purified on the non-phosphorylated peptide, yielding the antibody specific for non-phosphorylated Y595. Western blots were performed using antibodies against total ADAP (1:250, cat # F71620, BD Pharmingen), pY595 and non-pY595 ADAP (1:1000), FLAG (1:1000, F-1804 'M2', Sigma), GFP (1:2000, JL-8, detects most *Aequorea victoria* GFP variants, cat # 632381, Clontech), phosphotyrosine (pY) (1:2000, 4G.10, cat # 05-321, Millipore), pY783 PLCγ1 (1:1000, cat # 44-696G, Biosource, Cambridge, MA), goat anti-SKAP55 (1:1000, from Stefanie Kliche, Institute for Molecular and Clinical Immunology, Otto-von-Guericke-University, Magdeburg, Germany), SLP-76 (1:200, cat # AS55-P, Antibody Solutions, Sunnyvale, CA), pY145 SLP-76 (1:1000, cat # 2419-1, Sigma), γ-Tubulin (1:1000, cat # T3559, Sigma), pERK1/2 (1:5000, cat # V803A, Promega, Madison, WI, USA), ERK1 (1:5000, cat # 519002015, BD Pharmingen), PLCγ1 (1:1000, cat # 2822, Cell Signaling), and pY319 ZAP-70 (1:1000, cat # 2701S, Cell Signaling). Immunoprecipitations performed with antibodies against FLAG ('M2', Sigma), pY595 ADAP, and non-pY595 ADAP used 2.5 µg of antibody per reaction. Immunoprecipitations performed with antibodies against GFP (ab290, versus most *Aequorea victoria* GFP variants, Abcam) used 1 µg of antibody per reaction. Surface expression levels were assessed by flow cytometry using PE–Cy5-conjugated anti-CD69 (1:20, FN50, cat # 555532, BD Pharmingen) and Alexa-Fluor-647-conjugated anti-CD3 (1:20, UCHT1, cat # 557706, BD Pharmingen). Immunofluorescence studies were performed using Alexa-Fluor-647-conjugated antibodies specific for rabbit IgG (1:10,000, cat # A21245, Molecular Probes). For ADAP immunofluorescence, the pY595 serum was used at 1:25 and the non-phosphorylated Y595 serum at 1:50.

T cell stimulations and immunoprecipitations

T cells were stimulated with a 1:500 dilution of C305 ascites. Where indicated, T cells were concurrently treated with 1 µM pervanadate (equal concentrations of sodium orthovanadate+hydrogen peroxide). Stimulations were stopped at the indicated times by dilution into ice-cold PBS supplemented with 10 mM NaF and 1 mM Na_3VO_4, centrifuged, and lysed in ice cold buffer containing 20 mM Tris-HCl (pH 8.0), 150 mM NaCl, 1 mM EDTA, 1% Triton X-100, 10 mM NaF, 1 mM Na_3VO_4 and Complete protease inhibitor cocktail (Roche). After 10 min on ice, lysates were centrifuged at 4°C. For immunoprecipitations, cleared lysates were incubated with the indicated antibodies pre-bound to protein G or protein A beads (Thermo Fisher) for 1–2 h at room temperature.

Dynamic imaging and immunofluorescence

Cells were stimulated in glass-bottom 96-well plates as previously described (Bunnell et al., 2003; Sylvain et al., 2011). Imaging wells were pre-treated with 0.01% poly-L-Lysine, coated with 10 µg/ml OKT3, and blocked with 1% bovine serum albumin (BSA) in PBS. Live- and fixed-cell imaging runs were performed in cell culture medium supplemented with 25 mM Hepes (Cambrex Bio Science, East Rutherford, NJ). Live-cell imaging runs were acquired over at least 300 s. Confocal images were acquired with a Zeiss 200M microscope, 40× NA 1.3 Plan-Neofluar or 63× NA 1.4 Plan-Apochromat oil immersion objectives (Carl Zeiss AG, Jena, Germany), and a CSU-10 confocal spinning-disk head (Yokogawa Electric, Tokyo, Japan). Image capture was performed with an Orca ER CCD camera, an ORCA Flash 4.0 v2 camera (Hamamatsu Photonics, Hamamatsu City, Japan) or an XR MEGA-10 intensified CCD camera (Stanford Photonics, Palo Alto, CA). Images were acquired with Perkin-Elmer Ultraview or µManger software (Edelstein et al., 2010). Fluorescent protein detection was previously described (Bunnell et al., 2002).

Image processing

Image stacks were compiled using AppleScript (Apple Computer, Cupertino, CA) and iVision scripts (iVision, Atlanta, GA). Most image analysis was performed using iVision scripts (available upon request). However, 'standard deviation over time' images were produced using ImageJ (NIH) (Schneider et al., 2012). The iVision scripts used to quantify microcluster duration, half-life, movement, maximum sustained speed, SLP-76 clustering efficiency and boundary fluctuation were previously described (Sylvain et al., 2011; Ophir et al., 2013). To assess lamellipodial localization, iVision scripts were used to mask cells and SLP-76 microclusters using the 'Segmentation' tool. Ratiometric images were generated for the non-clustered regions of the cells using the 'Image Arithmetic' tool.

Contact formation and contact morphology assays

For contact formation assays, Jurkat T cells expressing the indicated fluorescent proteins were injected into imaging wells coated with or without 10 µg/ml OKT3, incubated at 37°C for 10 min, and fixed with 1% paraformaldehyde (PFA, Thermo Fisher). Two-step *z*-stacks were acquired to detect well-spread cells at the plane of contact (0 µm) and total cells in the viewing area (+5 µm). Multiple wells were examined for each condition. Contact formation is expressed as the percentage of cells that formed well-spread contacts. For contact morphology assays, T cells were stimulated as above, but were imaged dynamically, and synapse formation was scored as 'stable', 'fluctuating' or 'failed', based on the degree of spreading and the degree of movement at the boundary of the cell.

TCR adhesion assays

Briefly, T cells were labeled with 4 µM 2′,7′-bis(2-carboxyethyl), 5(and -6) carboxyfluorescein (BCECF, Molecular Probes) for 30 min at 37°C, as described previously (Ophir et al., 2013). For all assays, T cells were plated in glass-bottomed 96 well plates pre-treated with 0.01% poly-L-Lysine, left uncoated or coated with OKT3 (10 µg/ml), and blocked with 1% BSA in PBS. Cells were allowed to adhere for 30 min at 37°C and were vortexed and washed to remove unbound cells. BCECF fluorescence was read on a SpectraMax plate reader (Molecular Devices) at 488 nm excitation and 530 nm emission before and after vortexing. Results are presented as raw fractional retention.

CD69 and Ca^{2+} assays

TCR-induced increases in surface CD69 and intracellular Ca^{2+} were measured by flow cytometry. In all cases, J14 cells were transfected or transduced with vectors encoding either mYFP or SLP-76.mYFP chimeras. For CD69 assays, transfected cells were stimulated with 10 ng/ml soluble OKT3 or with plate-bound OKT3 (coated at 10 µg/ml) for 16-24 h at 37°C. Mean fluorescence intensities (MFI) are shown for cells expressing matched levels of YFP. For Ca^{2+} assays J14 cells were transfected with SLP-76.mYFP chimeras, stained with 10 µM Indo-1, and analyzed using a BD LSRII flow cytometer, as described previously (Sylvain et al., 2011). Basal Ca^{2+} levels were read for 2 min, at which point

OKT3 was added to 30 ng/ml and experimental Ca^{2+} levels were read for 10 min. Ionomycin was added to 10 µM, and peak Ca^{2+} levels were read for 3 min. Null, moderate and high subpopulations were identified by gating for mYFP expression. Ca^{2+} responses were normalized to the ionomycin-induced peak to enable comparisons between samples. Comparisons between subpopulations were performed by determining the percentage change in the area under the curve relative to the internal null population. All flow data were analyzed using FlowJo (version 8.8.7, FlowJo LLC, Ashland, OR) and Microsoft Excel.

Statistical considerations

Definition of sample size

For studies employing transient transfections, each experimental replicate involved an independent transfection. All stable lines of lentiviral origin were derived at least twice; in each case these independently derived lines yielded comparable results. Each experiment was performed on a separate day, using freshly prepared imaging plates. For analyses of SLP-76 microcluster behavior, at least three independent experiments were conducted per condition, with each experiment involving multiple cells. Statistical comparisons were performed using the number of experiments; the numbers of experiments and cells are reported in Tables S1–S3. Based on our own previous studies, perturbations of SLP-76 microclusters commonly yield normalized effect sizes ≥2. Under these conditions n=3 is sufficient to incorrectly reject the null hypothesis <5% of the time, with a power of 90%. Comparable effect sizes were observed here. Calculations performed using each cell as a replicate yielded similar conclusions (data not shown).

Inclusion and exclusion criteria

Pre-established inclusion criteria require that cell lines test as >70% CD3ε-positive within 1 week of use and that all cells for a given experimental condition must fall within a 3-fold range of brightness, given comparable power and exposure settings. Data were only excluded if positive controls performed at the beginning or end of session failed, indicating the presence of a technical defect.

Group allocation

Group allocation is not relevant to this study.

Extent of blinding

For verification, qualitative analyses were repeated by a researcher who was blind to the experimental condition. Quantitative analyses of microcluster movement were conducted using an analytical pipeline that presented kymographs for cluster tracking in a randomized order and without reference to the experimental manipulation.

Appropriateness of statistical tests

Samples were compared with a two-tailed Student's *t*-test for unpaired samples. The relevant measures of dispersion and precision are provided in Tables S1–S3 and figure legends. The standard deviation among the samples all fall within the same order of magnitude, and the microcluster data are normally distributed when examined across all cells.

Figure preparation

Figures and tables were compiled using Microsoft Excel, Microsoft Word, Microsoft PowerPoint, iVision, FlowJo and EZ Draw (Dekkora Optics, Poynette, WI, USA). Movies 1–17 were exported using iVision and compressed using Quicktime v10.4 (Apple Computer).

Acknowledgements

We thank M. A. Fray for many helpful discussions and his critical readings of the manuscript and K. Nguyen for his preliminary studies of ADAP. In addition, we recognize the W. M. Keck Foundation and the Eshe Fund for their generous support of core facilities at Tufts.

Competing interests

The authors declare no competing or financial interests.

Author contributions

Conceptualization: J.B.L., S.C.B.; Methodology: J.B.L., M.J.O., R.S., M.-C.S., S.C.B.; Software: F.A.S., M.J.O., S.C.B.; Validation: J.B.L., R.S., S.C.B.; Formal analysis: J.B.L., F.A.S., J.M.M., K.P.E., M.O.S., M.J.O., M.-C.S., S.C.B.; Investigation: J.B.L., F.A.S., J.M.M., K.P.E., M.O.S., M.J.O., M.-C.S., S.C.B.; Resources: R.S., S.C.B.; Data curation: J.B.L., F.A.S., J.M.M., K.P.E., M.O.S., M.J.O., S.C.B.; Writing - original draft: J.B.L., F.A.S., S.C.B.; Writing - review & editing: J.B.L., F.A.S., J.M.M., K.P.E., M.J.O., M.-C.S., S.C.B.; Visualization: J.B.L., F.A.S., S.C.B.; Supervision: M.-C.S., S.C.B.; Project administration: S.C.B.; Funding acquisition: S.C.B.

Funding

This work was supported by a Brain and Immuno-Imaging Award from the Dana Foundation, a Scientist Development Grant from the American Heart Association (0635546T), and a grant from the National Institute of Allergy and Infectious Diseases (NIH R01 AI076575-01). J.B.L. was supported by a pre-doctoral NRSA from the National Cancer Institute (F31CA136153). K.P.E and M.J.O. received support from NIH T32 AI007077; F.A.S. received support from NIH T32 GM008448. Deposited in PMC for release after 12 months.

Supplementary information

Supplementary information available online at
http://jcs.biologists.org/lookup/doi/10.1242/jcs.215517.supplemental

References

Acuto, O., Di Bartolo, V. and Michel, F. (2008). Tailoring T-cell receptor signals by proximal negative feedback mechanisms. *Nat. Rev. Immunol.* **8**, 699-712.

Baker, R. G., Hsu, C. J., Lee, D., Jordan, M. S., Maltzman, J. S., Hammer, D. A., Baumgart, T. and Koretzky, G. A. (2009). The adapter protein SLP-76 mediates "outside-in" integrin signaling and function in T cells. *Mol. Cell. Biol.* **29**, 5578-5589.

Balagopalan, L., Barr, V. A., Sommers, C. L., Barda-Saad, M., Goyal, A., Isakowitz, M. S. and Samelson, L. E. (2007). c-Cbl-mediated regulation of LAT-nucleated signaling complexes. *Mol. Cell. Biol.* **27**, 8622-8636.

Balagopalan, L., Ashwell, B. A., Bernot, K. M., Akpan, I. O., Quasba, N., Barr, V. A. and Samelson, L. E. (2011). Enhanced T-cell signaling in cells bearing linker for activation of T-cell (LAT) molecules resistant to ubiquitylation. *Proc. Natl. Acad. Sci. USA* **108**, 2885-2890.

Barr, V. A., Balagopalan, L., Barda-Saad, M., Polishchuk, R., Boukari, H., Bunnell, S. C., Bernot, K. M., Toda, Y., Nossal, R. and Samelson, L. E. (2006). T-cell antigen receptor-induced signaling complexes: internalization via a cholesterol-dependent endocytic pathway. *Traffic* **7**, 1143-1162.

Boerth, N. J., Sadler, J. J., Bauer, D. E., Clements, J. L., Gheith, S. M. and Koretzky, G. A. (2000). Recruitment of SLP-76 to the membrane and glycolipid-enriched membrane microdomains replaces the requirement for linker for activation of T cells in T cell receptor signaling. *J. Exp. Med.* **192**, 1047-1058.

Braiman, A., Barda-Saad, M., Sommers, C. L. and Samelson, L. E. (2006). Recruitment and activation of PLCγ1 in T cells: a new insight into old domains. *EMBO J.* **25**, 774-784.

Bunnell, S. C. (2010). Multiple microclusters: diverse compartments within the immune synapse. *Curr. Top. Microbiol. Immunol.* **340**, 123-154.

Bunnell, S. C., Kapoor, V., Trible, R. P., Zhang, W. and Samelson, L. E. (2001). Dynamic actin polymerization drives T cell receptor-induced spreading: a role for the signal transduction adaptor LAT. *Immunity* **14**, 315-329.

Bunnell, S. C., Hong, D. I., Kardon, J. R., Yamazaki, T., Mcglade, C. J., Barr, V. A. and Samelson, L. E. (2002). T cell receptor ligation induces the formation of dynamically regulated signaling assemblies. *J. Cell Biol.* **158**, 1263-1275.

Bunnell, S. C., Barr, V. A., Fuller, C. L. and Samelson, L. E. (2003). High-resolution multicolor imaging of dynamic signaling complexes in T cells stimulated by planar substrates. *Sci. STKE* **2003**, PL8.

Bunnell, S. C., Singer, A. L., Hong, D. I., Jacque, B. H., Jordan, M. S., Seminario, M.-C., Barr, V. A., Koretzky, G. A. and Samelson, L. E. (2006). Persistence of cooperatively stabilized signaling clusters drives T-cell activation. *Mol. Cell. Biol.* **26**, 7155-7166.

Burbach, B. J., Srivastava, R., Medeiros, R. B., O'gorman, W. E., Peterson, E. J. and Shimizu, Y. (2008). Distinct regulation of integrin-dependent T cell conjugate formation and NF-κB activation by the adapter protein ADAP. *J. Immunol.* **181**, 4840-4851.

Burbach, B. J., Srivastava, R., Ingram, M. A., Mitchell, J. S. and Shimizu, Y. (2011). The Pleckstrin homology domain in the SKAP55 adapter protein defines the ability of the adapter protein ADAP to regulate integrin function and NF-κB activation. *J. Immunol.* **186**, 6227-6237.

Burns, J. C., Corbo, E., Degen, J., Gohil, M., Anterasian, C., Schraven, B., Koretzky, G. A., Kliche, S. and Jordan, M. S. (2011). The SLP-76 Src homology 2 domain is required for T cell development and activation. *J. Immunol.* **187**, 4459-4466.

Cai, E., Marchuk, K., Beemiller, P., Beppler, C., Rubashkin, M. G., Weaver, V. M., Gerard, A., Liu, T. L., Chen, B. C., Betzig, E. et al. (2017). Visualizing dynamic microvillar search and stabilization during ligand detection by T cells. *Science* **356**, eaal3118.

Chiang, J. and Hodes, R. J. (2011). Cbl enforces Vav1 dependence and a restricted pathway of T cell development. *PLoS ONE* **6**, e18542.

Chiang, Y. J., Sommers, C. L., Jordan, M. S., Gu, H., Samelson, L. E., Koretzky, G. A. and Hodes, R. J. (2004). Inactivation of c-Cbl reverses neonatal lethality and T cell developmental arrest of SLP-76-deficient mice. *J. Exp. Med.* **200**, 25-34.

Chiang, Y. J., Jordan, M. S., Horai, R., Schwartzberg, P. L., Koretzky, G. A. and Hodes, R. J. (2009). Cbl enforces an SLP76-dependent signaling pathway for T cell differentiation. *J. Biol. Chem.* **284**, 4429-4438.

Coussens, N. P., Hayashi, R., Brown, P. H., Balagopalan, L., Balbo, A., Akpan, I., Houtman, J. C. D., Barr, V. A., Schuck, P., Appella, E. et al. (2013). Multipoint binding of the SLP-76 SH2 domain to ADAP is critical for oligomerization of SLP-76 signaling complexes in stimulated T cells. *Mol. Cell. Biol.* **33**, 4140-4151.

da Silva, A. J., Li, Z., De Vera, C., Canto, E., Findell, P. and Rudd, C. E. (1997a). Cloning of a novel T-cell protein FYB that binds FYN and SH2-domain-containing leukocyte protein 76 and modulates interleukin 2 production. *Proc. Natl. Acad. Sci. USA* **94**, 7493-7498.

da Silva, A. J., Rosenfield, J. M., Mueller, I., Bouton, A., Hirai, H. and Rudd, C. E. (1997b). Biochemical analysis of p120/130: a protein-tyrosine kinase substrate restricted to T and myeloid cells. *J. Immunol.* **158**, 2007-2016.

di Bartolo, V., Montagne, B., Salek, M., Jungwirth, B., Carrette, F., Fourtane, J., Sol-Foulon, N., Michel, F., Schwartz, O., Lehmann, W. D. et al. (2007). A novel pathway down-modulating T cell activation involves HPK-1–dependent recruitment of 14-3-3 proteins on SLP-76. *J. Exp. Med.* **204**, 681-691.

Edelstein, A., Amodaj, N., Hoover, K., Vale, R. and Stuurman, N. (2010). Computer control of microscopes using microManager. *Curr. Protoc. Mol. Biol.* Chapter 14, Unit14 20.

Geng, L., Raab, M. and Rudd, C. (1999). Cutting edge: SLP-76 cooperativity with FYB/FYN-T in the up-regulation of TCR driven IL-2 transcription requires SLP-76 binding to FYB at Tyr595 and Tyr651. *J. Immunol.* **163**, 5753-5757.

Griffiths, E. K., Krawczyk, C., Kong, Y. Y., Raab, M., Hyduk, S. J., Bouchard, D., Chan, V. S., Kozieradzki, I., Oliveira-Dos-Santos, A. J., Wakeham, A. et al. (2001). Positive regulation of T cell activation and integrin adhesion by the adapter Fyb/Slap. *Science* **293**, 2260-2263.

Hashimoto-Tane, A., Sakuma, M., Ike, H., Yokosuka, T., Kimura, Y., Ohara, O. and Saito, T. (2016). Micro-adhesion rings surrounding TCR microclusters are essential for T cell activation. *J. Exp. Med.* **213**, 1609-1625.

Heuer, K., Arbuzova, A., Strauss, H., Kofler, M. and Freund, C. (2005). The helically extended SH3 domain of the T cell adaptor protein ADAP is a novel lipid interaction domain. *J. Mol. Biol.* **348**, 1025-1035.

Heuer, K., Sylvester, M., Kliche, S., Pusch, R., Thiemke, K., Schraven, B. and Freund, C. (2006). Lipid-binding hSH3 domains in immune cell adapter proteins. *J. Mol. Biol.* **361**, 94-104.

Houtman, J. C. D., Yamaguchi, H., Barda-Saad, M., Braiman, A., Bowden, B., Appella, E., Schuck, P. and Samelson, L. E. (2006). Oligomerization of signaling complexes by the multipoint binding of GRB2 to both LAT and SOS1. *Nat. Struct. Mol. Biol.* **13**, 798-805.

Huang, Y., Norton, D. D., Precht, P., Martindale, J. L., Burkhardt, J. K. and Wange, R. L. (2005). Deficiency of ADAP/Fyb/SLAP-130 destabilizes SKAP55 in Jurkat T cells. *J. Biol. Chem.* **280**, 23576-23583.

Huse, M., Klein, L. O., Girvin, A. T., Faraj, J. M., Li, Q.-J., Kuhns, M. S. and Davis, M. M. (2007). Spatial and temporal dynamics of T cell receptor signaling with a photoactivatable agonist. *Immunity* **27**, 76-88.

Kasirer-Friede, A., Kang, J., Kahner, B., Ye, F., Ginsberg, M. H. and Shattil, S. J. (2014). ADAP interactions with talin and kindlin promote platelet integrin αIIbβ3 activation and stable fibrinogen binding. *Blood* **123**, 3156-3165.

Kliche, S., Breitling, D., Togni, M., Pusch, R., Heuer, K., Wang, X., Freund, C., Kasirer-Friede, A., Menasche, G. and Koretzky, G. A. (2006). The ADAP/SKAP55 signaling module regulates T-cell receptor-mediated integrin activation through plasma membrane targeting of Rap1. *Mol. Cell. Biol.* **26**, 7130-7144.

Kliche, S., Worbs, T., Wang, X., Degen, J., Patzak, I., Meineke, B., Togni, M., Moser, M., Reinhold, A., Kiefer, F. et al. (2012). CCR7-mediated LFA-1 functions in T cells are regulated by 2 independent ADAP/SKAP55 modules. *Blood* **119**, 777-785.

Krause, M., Sechi, A. S., Konradt, M., Monner, D., Gertler, F. B. and Wehland, J. (2000). Fyn-binding protein (Fyb)/SLP-76-associated protein (SLAP), Ena/vasodilator-stimulated phosphoprotein (VASP) proteins and the Arp2/3 complex link T cell receptor (TCR) signaling to the actin cytoskeleton. *J. Cell Biol.* **149**, 181-194.

Krawczyk, C., Bachmaier, K., Sasaki, T., Jones, R. G., Snapper, S. B., Bouchard, D., Kozieradzki, I., Ohashi, P. S., Alt, F. W. and Penninger, J. M. (2000). Cbl-b is a negative regulator of receptor clustering and raft aggregation in T cells. *Immunity* **13**, 463-473.

Kwon, J., Qu, C.-K., Maeng, J.-S., Falahati, R., Lee, C. and Williams, M. S. (2005). Receptor-stimulated oxidation of SHP-2 promotes T-cell adhesion through SLP-76-ADAP. *EMBO J.* **24**, 2331-2341.

Lange, S., Sylvester, M., Schümann, M., Freund, C. and Krause, E. (2010). Identification of phosphorylation-dependent interaction partners of the adapter protein ADAP using quantitative mass spectrometry: SILAC vs (18)O-labeling. *J. Proteome Res.* **9**, 4113-4122.

Lasserre, R., Cuche, C., Blecher-Gonen, R., Libman, E., Biquand, E., Danckaert, A., Yablonski, D., Alcover, A. and Di Bartolo, V. (2011). Release of serine/threonine-phosphorylated adaptors from signaling microclusters down-regulates T cell activation. *J. Cell Biol.* **195**, 839-853.

Lehmann, R., Meyer, J., Schuemann, M., Krause, E. and Freund, C. (2009). A novel S3S-TAP-tag for the isolation of T-cell interaction partners of adhesion and degranulation promoting adaptor protein. *Proteomics* **9**, 5288-5295.

Liu, H., Thaker, Y. R., Stagg, L., Schneider, H., Ladbury, J. E. and Rudd, C. E. (2013). SLP-76 sterile alpha motif (SAM) and individual H5 alpha helix mediate oligomer formation for microclusters and T-cell activation. *J. Biol. Chem.* **288**, 29539-29549.

Lugassy, J., Corso, J., Beach, D., Petrik, T., Oellerich, T., Urlaub, H. and Yablonski, D. (2015). Modulation of TCR responsiveness by the Grb2-family adaptor, Gads. *Cell. Signal.* **27**, 125-134.

Medeiros, R. B., Burbach, B. J., Mueller, K. L., Srivastava, R., Moon, J. J., Highfill, S., Peterson, E. J. and Shimizu, Y. (2007). Regulation of NF-κB activation in T cells via association of the adapter proteins ADAP and CARMA1. *Science* **316**, 754-758.

Menasche, G., Kliche, S., Chen, E. J. H., Stradal, T. E. B., Schraven, B. and Koretzky, G. (2007). RIAM links the ADAP/SKAP-55 signaling module to Rap1, facilitating T-cell-receptor-mediated integrin activation. *Mol. Cell. Biol.* **27**, 4070-4081.

Mitchell, J. S., Burbach, B. J., Srivastava, R., Fife, B. T. and Shimizu, Y. (2013). Multistage T cell-dendritic cell interactions control optimal CD4 T cell activation through the ADAP-SKAP55-signaling module. *J. Immunol.* **191**, 2372-2383.

Miura-Shimura, Y., Duan, L., Rao, N. L., Reddi, A. L., Shimura, H., Rottapel, R., Druker, B. J., Tsygankov, A., Band, V. and Band, H. (2003). Cbl-mediated ubiquitinylation and negative regulation of Vav. *J. Biol. Chem.* **278**, 38495-38504.

Mueller, K. L., Thomas, M. S., Burbach, B. J., Peterson, E. J. and Shimizu, Y. (2007). Adhesion and degranulation-promoting adapter protein (ADAP) positively regulates T cell sensitivity to antigen and T cell survival. *J. Immunol.* **179**, 3559-3569.

Myung, P. S., Derimanov, G. S., Jordan, M. S., Punt, J. A., Liu, Q.-H., Judd, B. A., Meyers, E. E., Sigmund, C. D., Freedman, B. D. and Koretzky, G. A. (2001). Differential requirement for SLP-76 domains in T cell development and function. *Immunity* **15**, 1011-1026.

Nguyen, K., Sylvain, N. R. and Bunnell, S. C. (2008). T cell costimulation via the integrin VLA-4 inhibits the actin-dependent centralization of signaling microclusters containing the adaptor SLP-76. *Immunity* **28**, 810-821.

Ophir, M. J., Liu, B. C. and Bunnell, S. C. (2013). The N terminus of SKAP55 enables T cell adhesion to TCR and integrin ligands via distinct mechanisms. *J. Cell Biol.* **203**, 1021-1041.

Patzak, I. M., Königsberger, S., Suzuki, A., Mak, T. W. and Kiefer, F. (2010). HPK1 competes with ADAP for SLP-76 binding and via Rap1 negatively affects T-cell adhesion. *Eur. J. Immunol.* **40**, 3220-3225.

Pauker, M. H., Reicher, B., Fried, S., Perl, O. and Barda-Saad, M. (2011). Functional cooperation between the proteins Nck and ADAP is fundamental for actin reorganization. *Mol. Cell. Biol.* **31**, 2653-2666.

Pauker, M. H., Reicher, B., Joseph, N., Wortzel, I., Jakubowicz, S., Noy, E., Perl, O. and Barda-Saad, M. (2014). WASp family verprolin-homologous protein-2 (WAVE2) and Wiskott-Aldrich syndrome protein (WASp) engage in distinct downstream signaling interactions at the T cell antigen receptor site. *J. Biol. Chem.* **289**, 34503-34519.

Peterson, E. J. (2003). The TCR ADAPts to integrin-mediated cell adhesion. *Immunol. Rev.* **192**, 113-121.

Peterson, E. J., Woods, M. L., Dmowski, S. A., Derimanov, G., Jordan, M. S., Wu, J. N., Myung, P. S., Liu, Q. H., Pribila, J. T., Freedman, B. D. et al. (2001). Coupling of the TCR to integrin activation by Slap-130/Fyb. *Science* **293**, 2263-2265.

Raab, M., Kang, H., Da Silva, A., Zhu, X. and Rudd, C. E. (1999). FYN-T-FYB-SLP-76 interactions define a T-cell receptor ζ/CD3-mediated tyrosine phosphorylation pathway that up-regulates interleukin 2 transcription in T-cells. *J. Biol. Chem.* **274**, 21170-21179.

Raab, M., Wang, H., Lu, Y., Smith, X., Wu, Z., Strebhardt, K., Ladbury, J. E. and Rudd, C. E. (2010). T cell receptor "inside-out" pathway via signaling module SKAP1-RapL regulates T cell motility and interactions in lymph nodes. *Immunity* **32**, 541-556.

Reicher, B., Joseph, N., David, A., Pauker, M. H., Perl, O. and Barda-Saad, M. (2012). Ubiquitylation-dependent negative regulation of WASp is essential for actin cytoskeleton dynamics. *Mol. Cell. Biol.* **32**, 3153-3163.

Rudd, C. E. and Wang, H. (2003). Hematopoietic adaptors in T-cell signaling: potential applications to transplantation. *Am. J. Transplant.* **3**, 1204-1210.

Schneider, C. A., Rasband, W. S. and Eliceiri, K. W. (2012). NIH Image to ImageJ: 25 years of image analysis. *Nat. Methods* **9**, 671-675.

Seminario, M.-C. and Bunnell, S. C. (2008). Signal initiation in T-cell receptor microclusters. *Immunol. Rev.* **221**, 90-106.

Shan, X., Czar, M. J., Bunnell, S. C., Liu, P., Liu, Y., Schwartzberg, P. L. and Wange, R. L. (2000). Deficiency of PTEN in Jurkat T cells causes constitutive localization of Itk to the plasma membrane and hyperresponsiveness to CD3 stimulation. *Mol. Cell. Biol.* **20**, 6945-6957.

Shaner, N. C., Lin, M. Z., Mckeown, M. R., Steinbach, P. A., Hazelwood, K. L., Davidson, M. W. and Tsien, R. Y. (2008). Improving the photostability of bright monomeric orange and red fluorescent proteins. *Nat. Methods* **5**, 545-551.

Sherman, E., Barr, V., Manley, S., Patterson, G., Balagopalan, L., Akpan, I., Regan, C. K., Merrill, R. K., Sommers, C. L., Lippincott-Schwartz, J. et al. (2011). Functional nanoscale organization of signaling molecules downstream of the T cell antigen receptor. *Immunity* **35**, 705-720.

Sherman, E., Barr, V. A., Merrill, R. K., Regan, C. K., Sommers, C. L. and Samelson, L. E. (2016). Hierarchical nanostructure and synergy of multimolecular signalling complexes. *Nat. Commun.* **7**, 12161.

Shui, J.-W., Boomer, J. S., Han, J., Xu, J., Dement, G. A., Zhou, G. and Tan, T.-H. (2007). Hematopoietic progenitor kinase 1 negatively regulates T cell receptor signaling and T cell-mediated immune responses. *Nat. Immunol.* **8**, 84-91.

Singer, A. L., Bunnell, S. C., Obstfeld, A. E., Jordan, M. S., Wu, J. N., Myung, P. S., Samelson, L. E. and Koretzky, G. A. (2004). Roles of the proline-rich domain in SLP-76 subcellular localization and T cell function. *J. Biol. Chem.* **279**, 15481-15490.

Srivastava, R., Burbach, B. J. and Shimizu, Y. (2010). NF-κB activation in T cells requires discrete control of IκB kinase α/β (IKKα/β) phosphorylation and IKKγ ubiquitination by the ADAP adapter protein. *J. Biol. Chem.* **285**, 11100-11105.

Sylvain, N. R., Nguyen, K. and Bunnell, S. C. (2011). Vav1-mediated scaffolding interactions stabilize SLP-76 microclusters and contribute to antigen-dependent T cell responses. *Sci. Signal.* **4**, ra14.

Sylvester, M., Kliche, S., Lange, S., Geithner, S., Klemm, C., Schlosser, A., Großmann, A., Stelzl, U., Schraven, B., Krause, E. et al. (2010). Adhesion and degranulation promoting adapter protein (ADAP) is a central hub for phosphotyrosine-mediated interactions in T cells. *PLoS ONE* **5**, e11708.

Valitutti, S., Dessing, M., Aktories, K., Gallati, H. and Lanzavecchia, A. (1995). Sustained signaling leading to T cell activation results from prolonged T cell receptor occupancy. Role of T cell actin cytoskeleton. *J. Exp. Med.* **181**, 577-584.

Vardhana, S., Choudhuri, K., Varma, R. and Dustin, M. L. (2010). Essential role of ubiquitin and TSG101 protein in formation and function of the central supramolecular activation cluster. *Immunity* **32**, 531-540.

Varma, R., Campi, G., Yokosuka, T., Saito, T. and Dustin, M. L. (2006). T cell receptor-proximal signals are sustained in peripheral microclusters and terminated in the central supramolecular activation cluster. *Immunity* **25**, 117-127.

Veale, M., Raab, M., Li, Z., da Silva, A. J., Kraeft, S.-K., Weremowicz, S., Morton, C. C. and Rudd, C. E. (1999). Novel isoform of lymphoid adaptor FYN-T-binding protein (FYB-130) interacts with SLP-76 and up-regulates interleukin 2 production. *J. Biol. Chem.* **274**, 28427-28435.

Wang, H., Mccann, F. E., Gordan, J. D., Wu, X., Raab, M., Malik, T. H., Davis, D. M. and Rudd, C. E. (2004). ADAP-SLP-76 binding differentially regulates supramolecular activation cluster (SMAC) formation relative to T cell-APC conjugation. *J. Exp. Med.* **200**, 1063-1074.

Wang, H., Wei, B., Bismuth, G. and Rudd, C. E. (2009). SLP-76-ADAP adaptor module regulates LFA-1 mediated costimulation and T cell motility. *Proc. Natl. Acad. Sci. USA* **106**, 12436-12441.

Wang, X., Li, J. P., Chiu, L. L., Lan, J. L., Chen, D. Y., Boomer, J. and Tan, T. H. (2012). Attenuation of T cell receptor signaling by serine phosphorylation-mediated lysine-30 ubiquitination of SLP-76. *J. Biol. Chem.* **287**, 34091-34100.

Wiede, F., Shields, B. J., Chew, S. H., Kyparissoudis, K., Van Vliet, C., Galic, S., Tremblay, M. L., Russell, S. M., Godfrey, D. I. and Tiganis, T. (2011). T cell protein tyrosine phosphatase attenuates T cell signaling to maintain tolerance in mice. *J. Clin. Invest.* **121**, 4758-4774.

Wu, J. N., Gheith, S., Bezman, N. A., Liu, Q.-H., Fostel, L. V., Swanson, A. M., Freedman, B. D., Koretzky, G. A. and Peterson, E. J. (2006). Adhesion- and degranulation-promoting adapter protein is required for efficient thymocyte development and selection. *J. Immunol.* **176**, 6681-6689.

Yuan, M., Mogemark, L. and Fällman, M. (2005). Fyn binding protein, Fyb, interacts with mammalian actin binding protein, mAbp1. *FEBS Lett.* **579**, 2339.

Zacharias, D. A., Violin, J. D., Newton, A. C. and Tsien, R. Y. (2002). Partitioning of lipid-modified monomeric GFPs into membrane microdomains of live cells. *Science* **296**, 913-916.

Zipfel, P. A., Bunnell, S. C., Witherow, D. S., Gu, J. J., Chislock, E. M., Ring, C. and Pendergast, A. M. (2006). Role for the Abi/Wave protein complex in T cell receptor-mediated proliferation and cytoskeletal remodeling. *Curr. Biol.* **16**, 35-46.

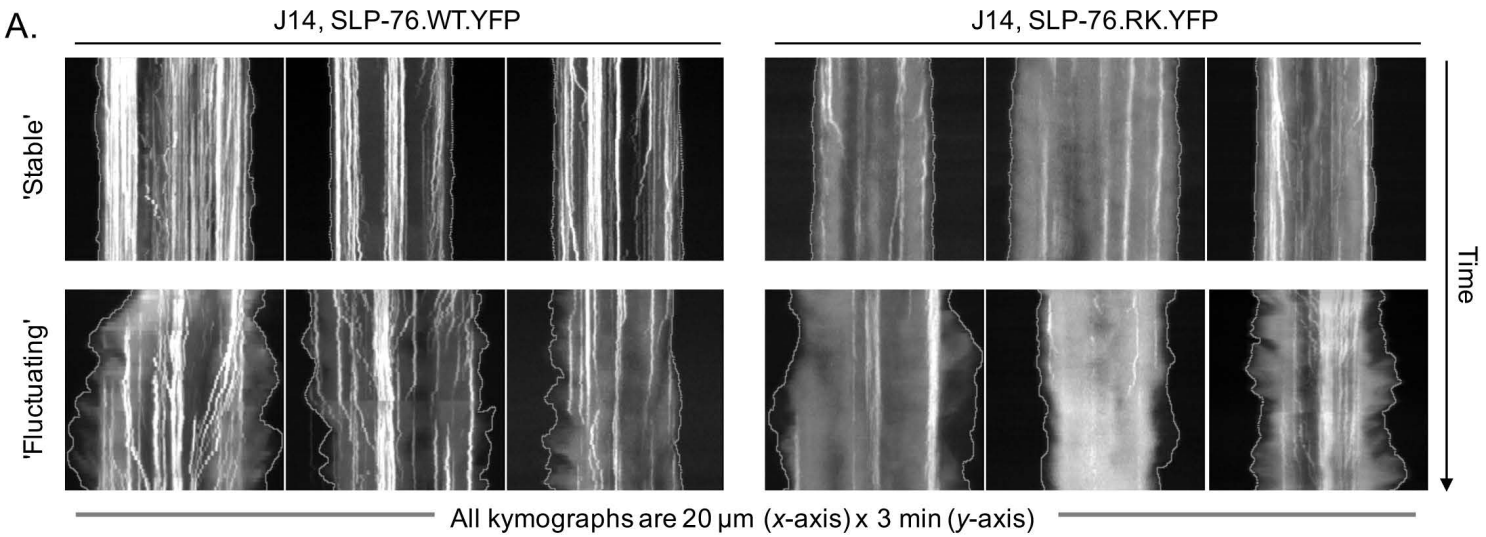

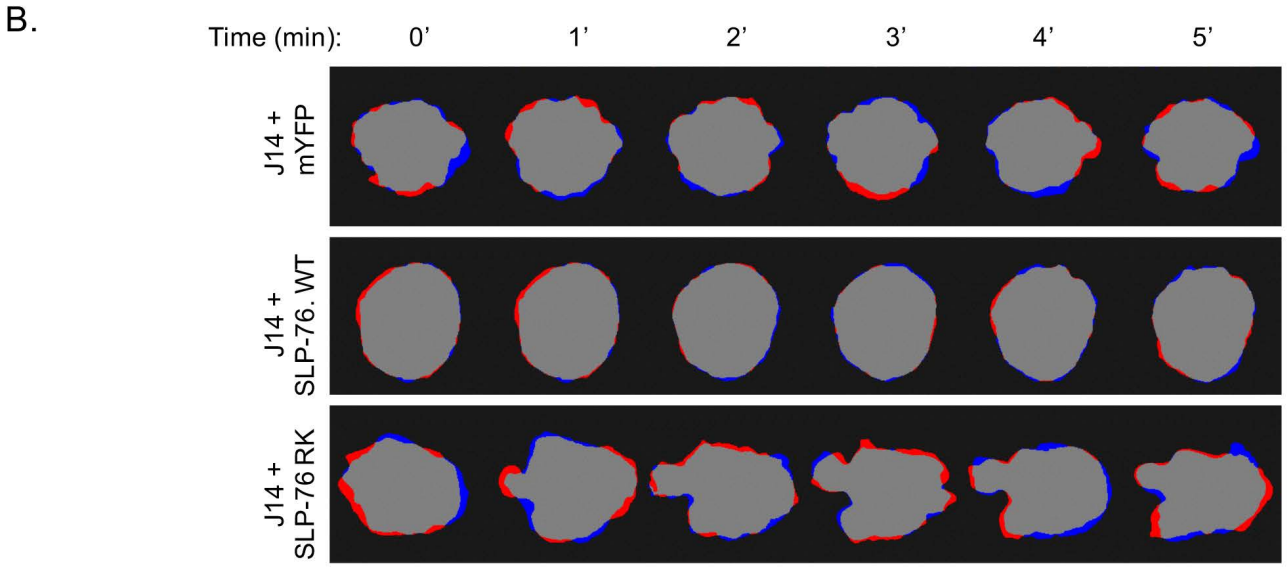

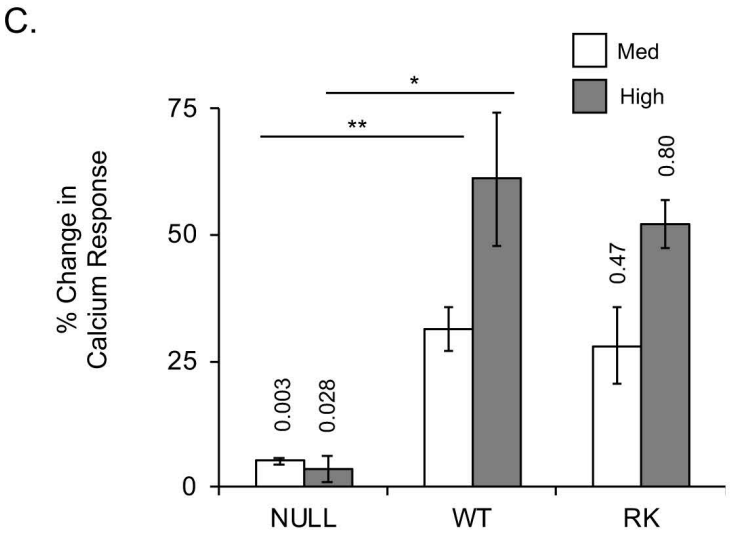

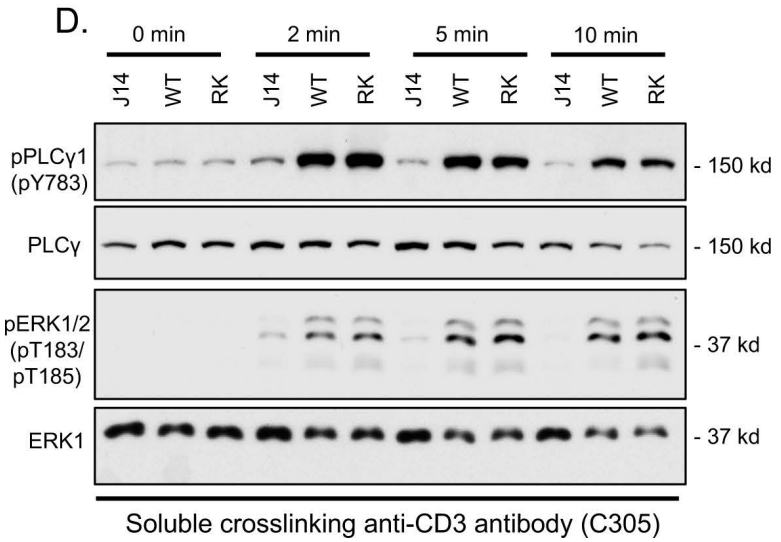

Figure S1. SLP-76 RK SH2 mutant impairs contact stability but is dispensable for calcium influx, PLCγ phosphorylation, and ERK1 activation. (A) SLP-76 deficient (J14) cells expressing WT human SLP-76.YFP or the SLP-76.RK.YFP SH2 mutant chimera were stimulated and imaged as in Figure 1. Kymographs depict movement within regions that encompass the entirety of the cell diameter over time (20 μm x 180 s). The contours of the cell contact are outlined in white and illustrate our scoring criteria for the "Stable" and "Fluctuating" cells tallied in Fig. 1E. **(B)** J14 cells expressing mYFP, WT SLP76, or a SH2 mutant SLP-76 were stimulated or imaged as above. Diagram indicates a time course representation of our boundary fluctuation quantification algorithm described in Ophir *et al* 2013. Briefly, areas of boundary growth are marked in blue, while areas of boundary contraction are marked in red. Boundary fluctuation was calculated in Fig. 1F by dividing the areas of red or blue fluctuation over the total cell area during the length of the movie. **(C)** J14 cells transiently expressing mYFP chimeras were assayed for TCR-induced Ca2+ entry (n=3 experiments). All errors are displayed as SEMs; p-values indicate significant differences from J14 cells expressing wild-type SLP-76.YFP (Student's two-tailed t-test for unpaired samples: *, $p < 0.05$; ** $p < 0.01$). **(D)** SLP-76 deficient J14 cells were lentivirally transduced with either WT SLP-76 or the SLP-76 RK SH2 mutant. Parental J14 and transduced cells were either left unstimulated or stimulated with C305 for 2 min, 5 min, or 10 min. Total lysates were western blotted as indicated (n=2 experiments).

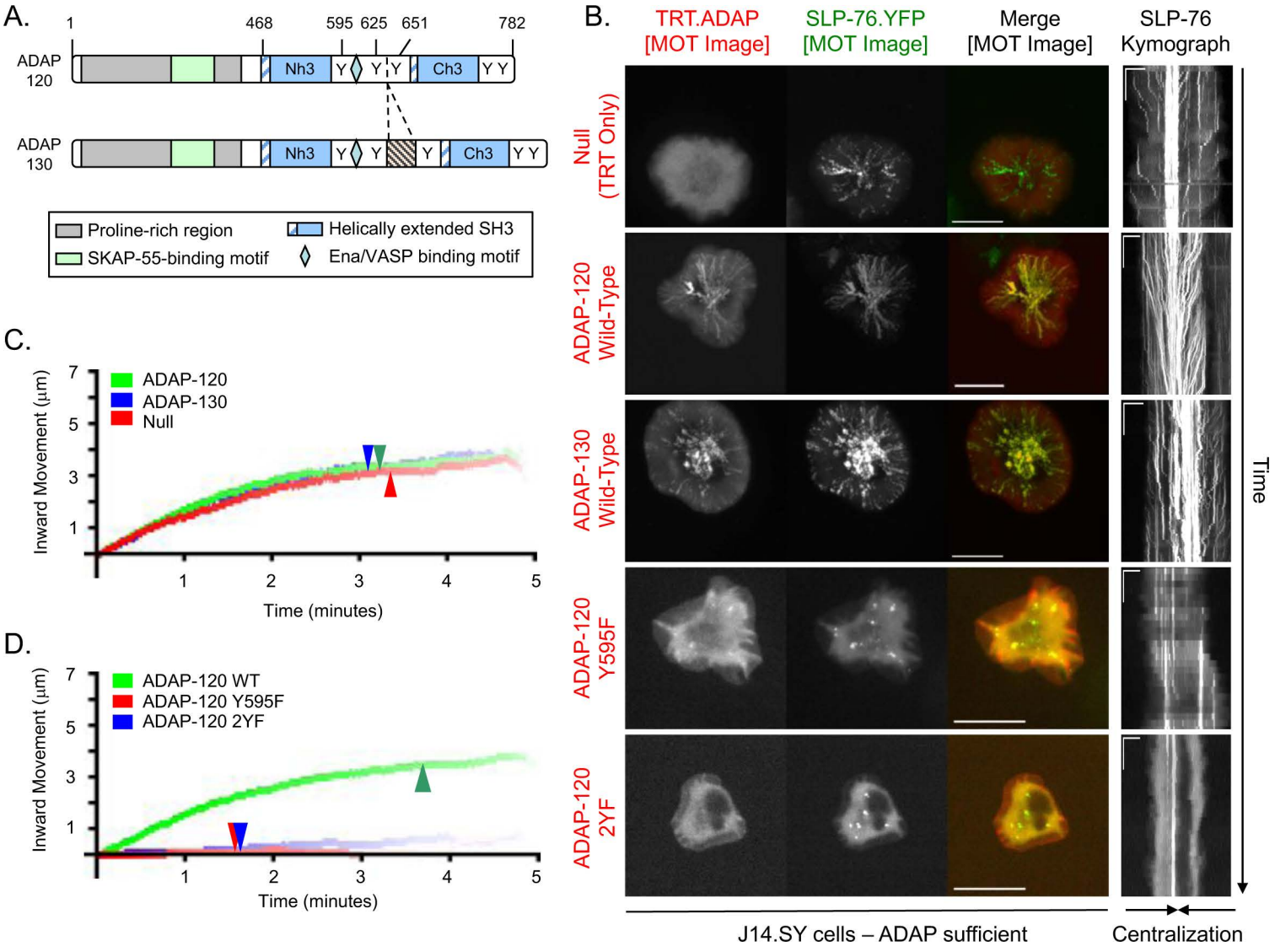

Figure S2. ADAP splice variants are recruited into persistent microclusters by SLP-76. **(A)** Domain structures of ADAP splice variants. For a diagram of the ADAP Y595F and 2YF tyrosine mutants see Figure 3A. **(B)** J14.SY cells transiently expressing either 3xFlag.TRT or the indicated 3xFlag.TRT.ADAP chimeras were stimulated and imaged as in Figure 1. MOT images were prepared from movies of SLP-76.YFP (green in merge) and 3xFlag.TRT (red in merge); kymographs were prepared from movies of SLP-76.YFP (see Figure 1 for descriptions of MOTs and kymographs). Scale bars are as in Figure 1B. **(C-D)** Composite kymographs depict average SLP-76 microcluster properties for conditions shown in (B), above. Microcluster properties, number of experiments, number of cells analyzed, and statistical comparisons are listed in Table S2.

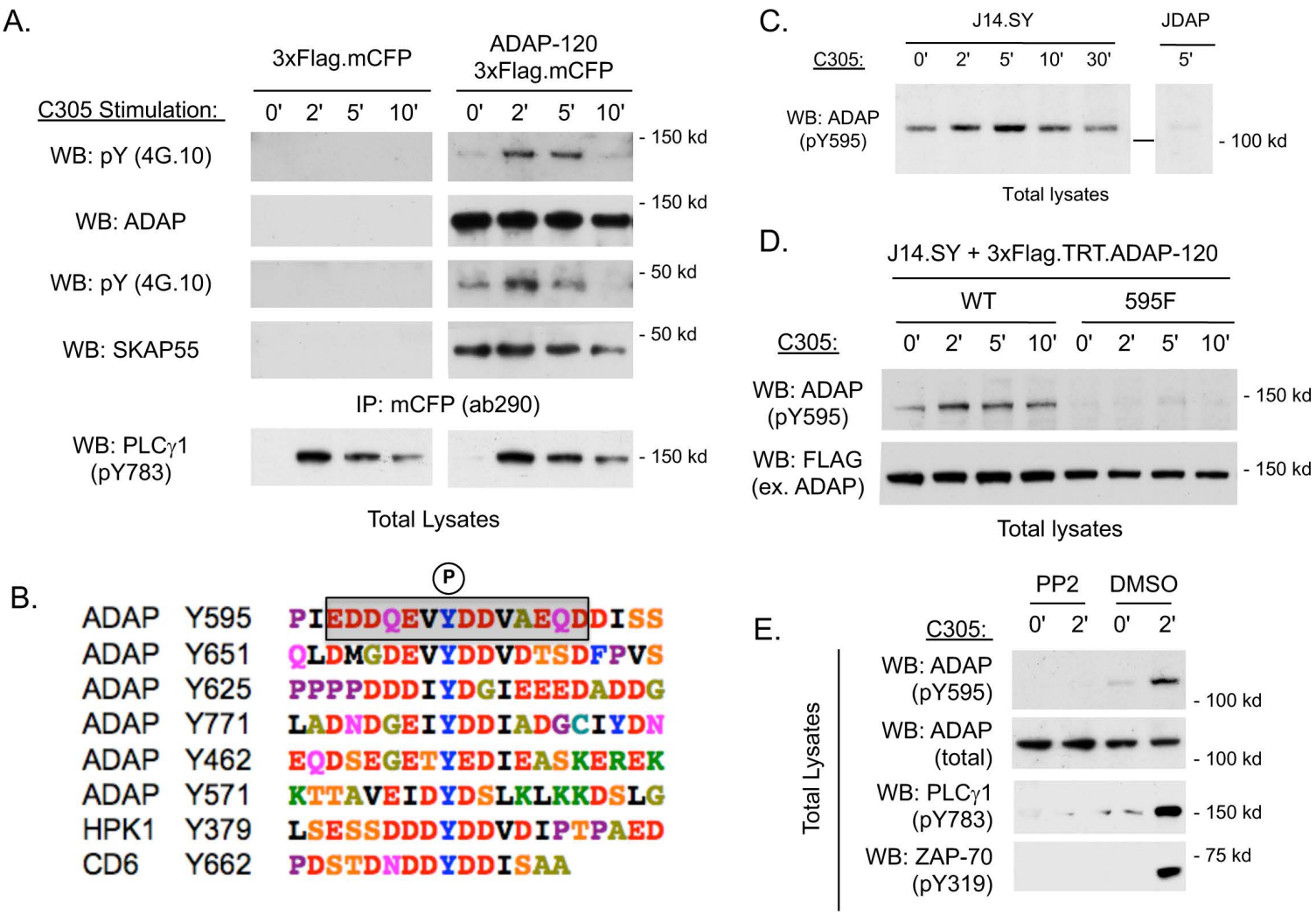

Figure S3. Validation of anti-ADAP pY595 antibody. (A) JDAP cells were transiently reconstituted with ADAP-120.3xFlag.mCFP, stimulated, and lysed. Exogenous ADAP was immunoprecipitated with anti-CFP (ab290) and western blotted as indicated. pY783 PLCγ1 provides a control for TCR activation. **(B)** Alignments of putative SLP-76 SH2 domain-binding sites in *Homo sapiens* ADAP-120, HPK1, and CD6. Antisera targeting ADAP pY595 were raised in rabbits and affinity purified using the boxed phosphopeptide. **(C)** To evaluate the kinetics of ADAP pY595 phosphorylation, J14.SY and JDAP cells were stimulated with C305 and western blotted for ADAP pY595. **(D)** J14.SY cells stably expressing either 3xFlag.TRT.ADAP-120.WT or 3xFlag.TRT.ADAP-120.595F chimeras were stimulated with C305, lysed, and western blotted for ADAP pY595. FLAG blot demonstrates even expression of the exogenous construct. **(E)** J14.SY cells were pre-treated with 10 μM PP2 or with DMSO carrier for 10 min prior to stimulation with C305. Total lysates were blotted as indicated (n=2). pY319 ZAP-70 and pY783 PLCγ1 provide controls for TCR activation. All western blots are representative of two or more independent experiments.

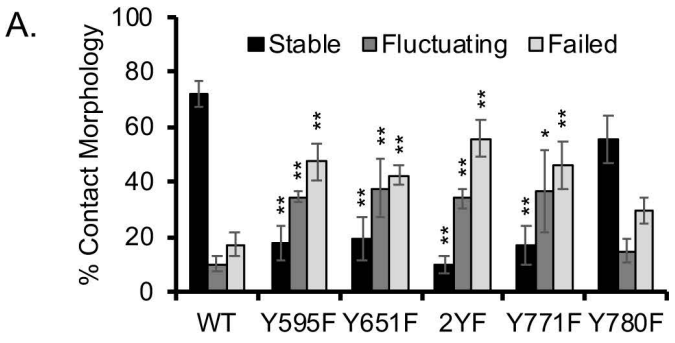

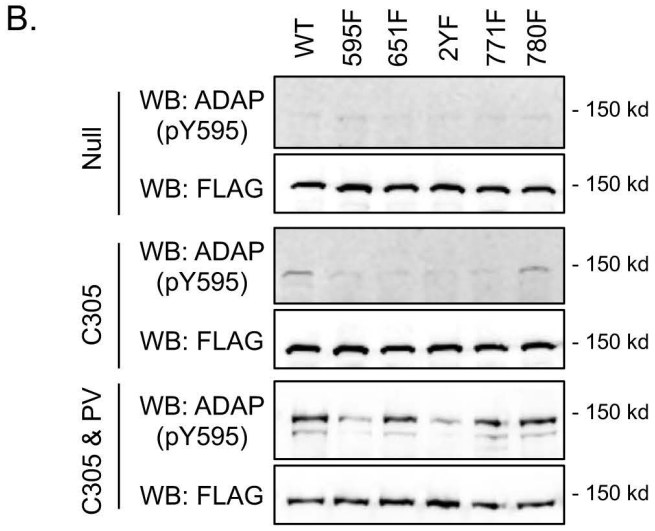

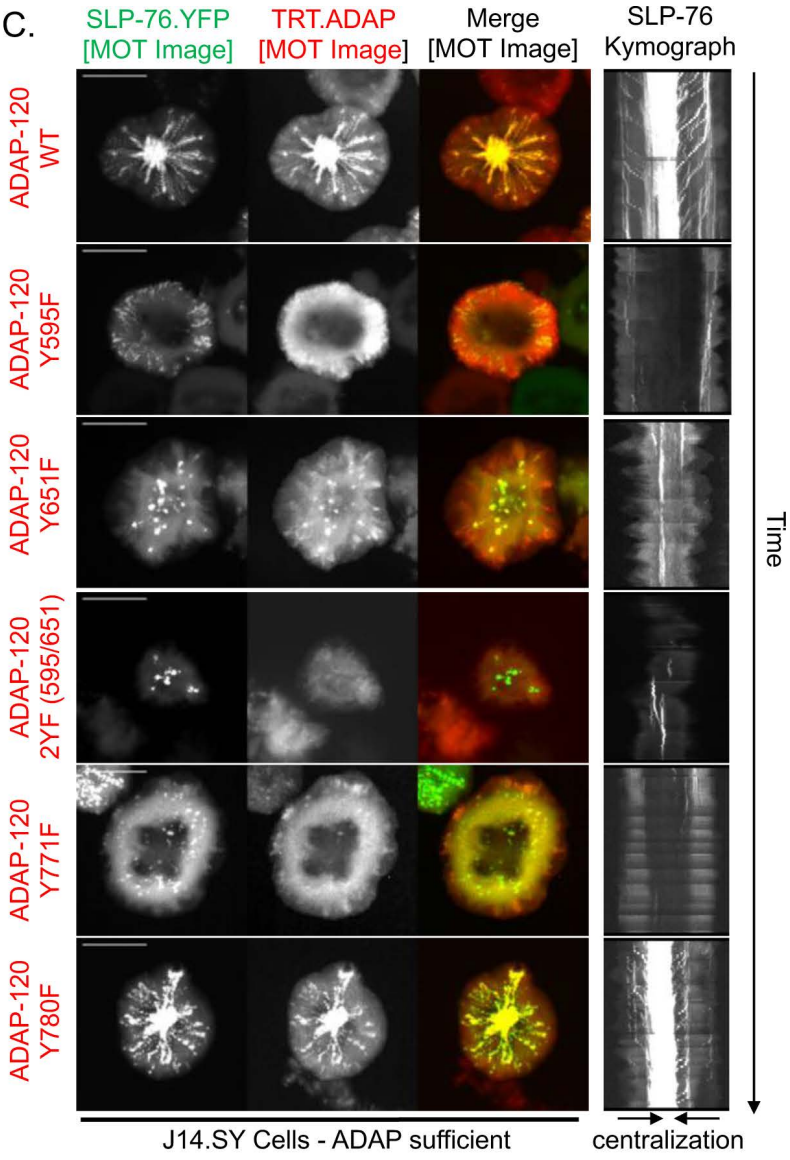

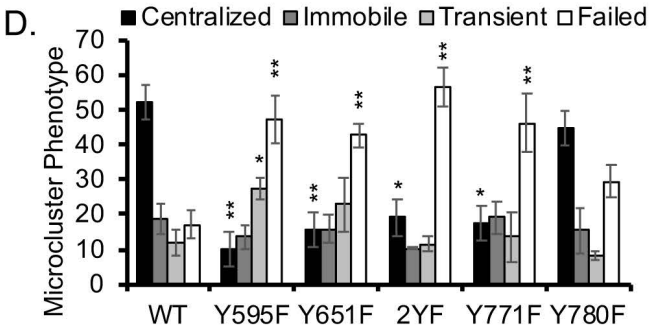

E.

ADAP Chimera	Replicates: cells	Replicates: wells
WT ADAP	246	8
Y595F	152	3
Y651	160	3
2YF	79	2
Y771F	130	3
Y780F	213	5

	Contact Morphology					
	Stable		Fluctuating		Failed	
ADAP Chimera	Mean +/- SEM	p vs. WT	Mean +/- SEM	p vs. WT	Mean +/- SEM	p vs. WT
WT ADAP	72.2 ± 5.0	1.00000	10.4 ± 3.1	1.00000	17.4 ± 4.2	1.00000
Y595F	18.1 ± 6.4	0.00012	34.5 ± 1.9	0.00087	47.4 ± 6.8	0.00250
Y651	19.5 ± 8.0	0.00018	37.9 ± 10.4	0.00280	42.6 ± 3.5	0.00469
2YF	10.0 ± 3.0	0.00022	34.1 ± 3.5	0.00463	55.9 ± 6.6	0.00172
Y771F	17.1 ± 6.9	0.00011	36.7 ± 15.2	0.01213	46.2 ± 8.5	0.00424
Y780F	55.5 ± 8.5	0.07145	15.1 ± 4.4	0.34950	29.5 ± 4.8	0.06950

	Microcluster Phenotype									
	Central		Immobile		Erratic		Transient		Failed	
ADAP Chimera	Mean +/- SEM	p vs. WT	Mean +/- SEM	p vs. WT	Mean +/- SEM	p vs. WT	Mean +/- SEM	p vs. WT	Mean +/- SEM	p vs. WT
WT ADAP	51.9 ± 6.8	1.00000	18.7 ± 4.3	1.00000	0.3 ± 0.3	1.00000	12.0 ± 3.8	1.00000	17.1 ± 4.0	1.00000
Y595F	10.3 ± 1.6	0.00372	13.5 ± 3.6	0.47429	1.5 ± 1.0	0.09564	27.4 ± 2.8	0.03465	47.4 ± 6.8	0.00198
Y651	15.7 ± 1.9	0.00823	15.9 ± 3.9	0.70231	3.0 ± 2.7	0.07073	22.8 ± 7.6	0.15605	42.6 ± 3.5	0.00365
2YF	19.1 ± 8.4	0.04059	10.3 ± 0.4	0.34625	2.6 ± 0.1	0.00330	11.6 ± 2.2	0.95443	56.5 ± 5.7	0.00118
Y771F	17.3 ± 5.6	0.01186	19.1 ± 4.8	0.95749	3.8 ± 3.5	0.05767	13.5 ± 7.3	0.83363	46.2 ± 8.5	0.00345
Y780F	44.5 ± 1.8	0.38813	15.4 ± 6.5	0.64533	2.4 ± 1.7	0.10586	8.2 ± 1.4	0.43563	29.5 ± 4.8	0.05822

Figure S4: ADAP tyrosines 595, 651, and 771 are essential and are functionally equivalent. J14.SY cells were stably transduced with the indicated 3xFlag.TRT.ADAP-120 chimeras. **(A)** Cells were visualized for 5 minutes while responding to OKT3-coated glass surfaces. Contact formation and morphology were manually scored for all ADAP-expressing cells in the imaging field. **(B)** Transduced cells were left unstimulated, stimulated with C305 for 2 minutes, or stimulated with C305 and pervanadate for 10 minutes. Total lysates were western blotted as indicated. **(C)** Image stacks captured in (A) were used to generate maximum over time (MOT) images and kymographs spanning the entire imaging period **(D)** Microcluster phenotypes were manually scored for all cells imaged in (A). **(E)** Data, errors, numbers of independent wells, and p-values for panels (A) and (D). All errors are displayed as SEM of independent wells; p-values indicate significant differences from J14.SY cells expressing wild-type ADAP-120 (Student's two-tailed t-test for unpaired samples: *, $p < 0.05$; ** $p < 0.01$).

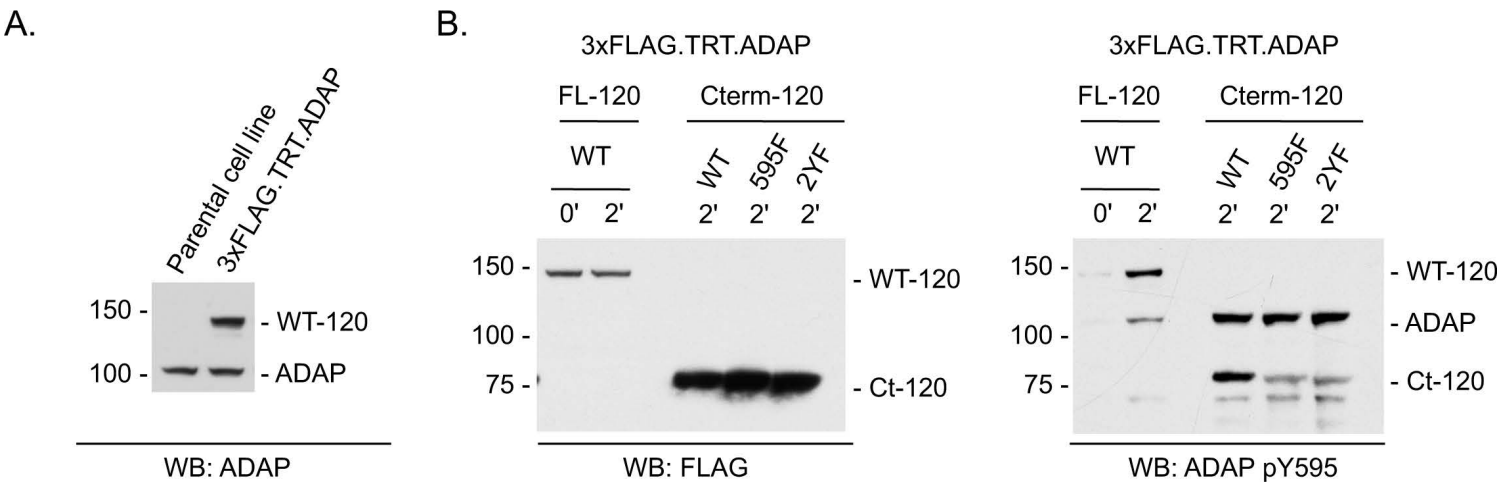

Figure S5. ADAP C-terminal tyrosine mutants do not support Y595 phosphorylation following TCR ligation. J14.SY cells were stably transduced with the wild-type 3xFlag.TRT.ADAP-120 chimera or with the indicated C-terminal chimeras. Lines expressing exogenous wild-type ADAP were sorted to obtain near-endogenous levels of protein, while the C-terminal lines were sorted for levels approximately 25-fold in excess of the endogenous protein. Cells were left unstimulated or stimulated for 2 minutes with C305; total lysates were analyzed by western blotting. **(A)** Total ADAP blots confirm that exogenous ADAP-120 (WT-120) is expressed at near-endogenous (ADAP) levels. **(B)** In conjunction with (A), anti-FLAG (left) and anti-ADAP pY595 (right) blots demonstrate that the wild-type C-terminal fragment (Ct-120) and endogenous ADAP are comparably phosphorylated despite the overexpression of this fragment relative to endogenous ADAP. All western blots are representative of three or more independent experiments.

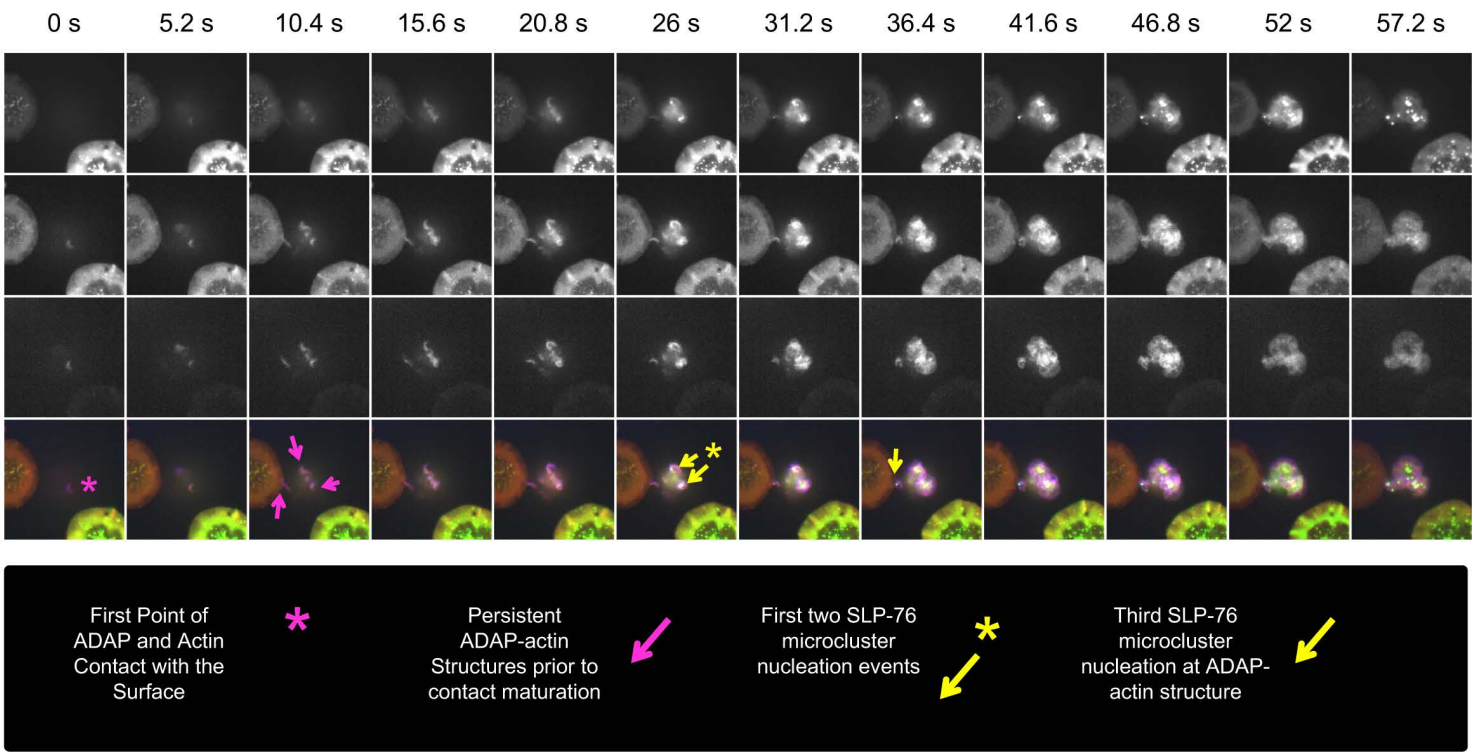

Figure S6: SLP-76 microclusters nucleate from ADAP and actin-enriched protrusions during T cell contact formation. J14.SY cells expressing 3xFlag.TRT.ADAP-120 were transiently transfected with mCFP.β-actin. The cells were stimulated and imaged as described in Figure 2. Representative images depict the first minute of cellular contact. Magenta arrowheads identify three different ADAP and actin-rich protrusive structures contacting the substrate. Yellow arrows emphasize subsequent SLP-76 microcluster formation on these cytoskeletal structures, with the yellow asterisks indicating the first microcluster nucleation events (n=2 experiments, 12 TRT.ADAP^{+} mCFP-β-actin^{+} J14.SY cells captured during contact formation).

Table S1. The SLP-76 SH2 domain contributes to SLP-76 microcluster persistence and movement.

SLP-76 chimeras	Persistence (s)	p *vs.* WT	Movement (µm)	p *vs.* WT	Max Speed (nm s^{-1})	p *vs.* WT	% SLP-76 in clusters	p *vs.* WT	*n* (exp)	*n* (cell)
SLP-76.WT *Hs*	218.9 ± 7.1	n.a.	4.05 ± 0.28	n.a.	116.9 ± 7.0	n.a.	57.1 ± 2.7	n.a.	6	46
SLP-76.RK *Hs*	**131.7 ± 24.4**	**6.4e-3**	**0.56 ± 0.04**	**1.7e-7**	**55.1 ± 3.9**	**1.6e-5**	**8.8 ± 2.0**	**5.6e-8**	6	45

Mm* vs. matched *Hs	Persistence (s)	p *vs.* *Hs*	Movement (µm)	p *vs.* *Hs*	Max Speed (nm s^{-1})	p *vs.* *Hs*	% SLP-76 in clusters	p *vs.* *Hs*	*n* (exp)	*n* (cell)
SLP-76.WT *Mm*	200.4 ± 13.3	0.22	3.77 ± 0.44	0.59	116.7 ± 8.9	0.98	48.5 ± 5.1	0.14	3	19
SLP-76.RK *Mm*	109.9 ± 8.6	0.56	0.52 ± 0.03	0.51	43.8 ± 1.1	0.09	11.5 ± 1.5	0.41	3	14

*(**Upper**)* J14 cells were transfected with SLP-76.WT or SLP-76.RK (see Figure 1). SLP-76 microcluster behavior was calculated from traces of individual microclusters from cells across the indicated number of experiments. Microcluster properties are shown ± SEM, based on the number of experiments; p values were calculated using a two-tailed Student's t-test for unpaired samples; significant differences from WT are shaded and in bold. *(**Lower**)* J14 cells were transfected with murine SLP-76.WT or SLP-76.RK. Microcluster behavior was calculated from traces of individual microclusters from cells across the indicated number of experiments. Microcluster properties are shown ± SEM, based on the number of experiments; p values were calculated versus the corresponding human chimeras using a two-tailed Student's t-test for unpaired samples; no significant differences were observed.

Table S2. ADAP is required for optimal SLP-76 microcluster movement and persistence.

ADAP chimeras	Persistence (s)	p *vs.* WT	p *vs.* TRT	Movement (μm)	p *vs.* WT	p *vs.* TRT	Max Speed (nm s^{-1})	p *vs.* WT	p *vs.* TRT	% SLP-76 in clusters	p *vs.* WT	p *vs.* TRT	*n* (exp)	*n* (cell)
TRT control	195.3 ± 10.0	0.87	n.a.	4.04 ± 0.35	0.76	n.a.	130.0 ± 6.5	0.91	n.a.	**56.2 ± 2.7**	**8.6e-4**	n.a.	7	30
120.WT	197.4 ± 7.3	n.a.	0.87	4.17 ± 0.21	n.a.	0.76	131.2 ± 6.9	n.a.	0.91	68.1 ± 1.5	n.a.	**8.6e-4**	15	69
130.WT	173.2 ± 12.4	0.18	0.25	3.48 ± 0.45	0.20	0.39	120.4 ± 12.5	0.52	0.49	62.7 ± 8.6	0.28	0.39	3	15
ADAP-KD	**83.4 ± 12.5**	**6.7e-6**	**4.1e-4**	**0.94 ± 0.02**	**5.6e-6**	**7.8e-4**	**61.5 ± 2.5**	**4.2e-4**	**3.0e-4**	**34.7 ± 4.2**	**1.9e-7**	**3.7e-3**	3	36
ADAP-KD/AB	196.9 ± 6.0	0.97	0.92	4.49 ± 0.30	0.53	0.47	139.6 ± 9.0	0.61	0.44	71.8 ± 3.2	0.33	**0.013**	3	30
120.Y595F	**137.8 ± 14.4**	**1.6e-3**	**0.011**	**0.80 ± 0.18**	**4.6e-7**	**1.7e-4**	**53.2 ± 6.9**	**3.2e-5**	**7.3e-5**	**29.6 ± 7.7**	**2.9e-7**	**5.6e-3**	4	29
120.2YF	**113.7 ± 9.3**	**3.5e-5**	**7.3e-4**	**0.60 ± 0.09**	**1.7e-7**	**8.8e-5**	**52.9 ± 5.5**	**2.8e-5**	**4.8e-5**	**19.6 ± 3.1**	**5.4e-11**	**3.1e-5**	4	25
120.Ct-WT	**126.6 ± 9.6**	**7.4e-5**	**1.1e-3**	**0.99 ± 0.04**	**1.1e-7**	**4.4e-5**	**65.1 ± 2.6**	**3.7e-5**	**2.1e-5**	**42.6 ± 4.5**	**1.5e-6**	**0.027**	5	47
120.Ct-595F	**157.9 ± 9.6**	**0.034**	0.064	3.15 ± 0.28	0.058	0.17	108.5 ± 10.5	0.18	0.12	**45.9 ± 5.8**	**6.5e-5**	0.11	3	12
120.Ct-2YF	169.6 ± 6.4	0.12	0.16	3.58 ± 0.28	0.26	0.45	135.7 ± 7.8	0.78	0.64	**54.4 ± 1.9**	**1.4e-3**	0.69	3	21
120.Ct-3YF	193.8 ± 3.4	0.83	0.93	4.18 ± 0.33	0.98	0.82	127.8 ± 15.2	0.84	0.88	61.9 ± 2.7	0.11	0.25	3	15

J14.SY cells were transfected with the indicated TRT expression vectors (see Figures 2, S2, and 5). SLP-76 microcluster behavior was calculated from traces of individual microclusters from cells across the indicated number of experiments. Microcluster properties are shown ± SEM, based on the number of experiments; p values were calculated using a two-tailed Student's t-test for unpaired samples; significant differences from wild-type ADAP-120 are shaded light orange and in bold; significant differences from the TRT control are shaded light purple and in bold.

Table S3. ADAP requires both Y595 and Y651 to stabilize SLP-76 microclusters.

ADAP chimeras	Persistence (s)	p *vs.* WT	p *vs.* TRT	Movement (μm)	p *vs.* WT	p *vs.* TRT	% SLP-76 in clusters	p *vs.* WT	p *vs.* TRT	*n* (exp)	*n* (cell)
TRT control	**70.0 ± 8.4**	**0.001**	n.a.	**7.8 ± 2.5**	**0.015**	n.a.	**21.7 ± 9.9**	**0.012**	n.a.	3	15
120.WT	185.6 ± 13.3	n.a.	**0.001**	34.7 ± 6.0	n.a.	**0.015**	65.5 ± 6.6	n.a.	**0.012**	4	22
120.Y595F	**112.3 ± 12.2**	**0.011**	**0.046**	**4.9 ± 0.2**	**0.008**	0.31	**20.2 ± 4.3**	**0.004**	0.90	3	15
120.2YF	**106.2 ± 3.6**	**0.004**	**0.017**	**9.0 ± 1.0**	**0.015**	0.69	**29.3 ± 6.3**	**0.012**	0.55	3	15
120.3YF	**83.7 ± 5.0**	**0.002**	0.24	**5.7 ± 1.1**	**0.009**	0.48	**24.0 ± 11.3**	**0.02**	0.89	3	17

JDAP cells were co-transfected with SLP-76 and the indicated TRT expression vectors (see Figure 3). SLP-76 microcluster behavior was calculated from traces of individual microclusters from cells across the indicated number of experiments. Microcluster properties are shown ± SEM, based on the number of experiments; p values were calculated using a two-tailed Student's t-test for unpaired samples; significant differences from wild-type ADAP-120 are shaded light orange and in bold; significant differences from the TRT control are shaded light purple and in bold.

SUPPLEMENTAL MOVIES.

All movies play back at 60x normal speed. All of the following movies are of cells that were stimulated on OKT3-coated cover slips and imaged continuously for 5 minutes.

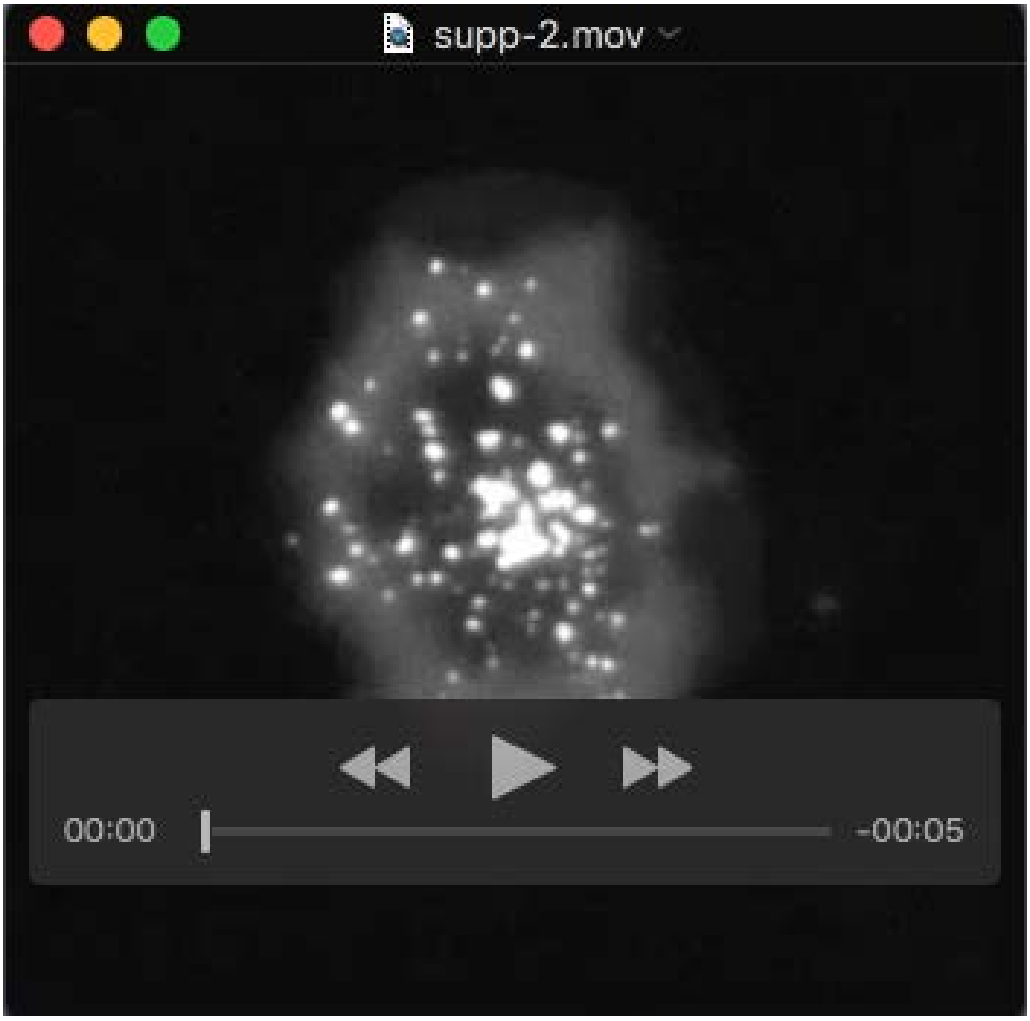

Movie S1. The SLP-76 SH2 domain regulates TCR-induced SLP-76 microcluster centralization and persistence (WT SLP-76 movie). SLP-76 deficient Jurkat T cells (J14 cells) were transiently transfected with an expression vector for a wild-type (WT) SLP-76.YFP chimera of human origin.

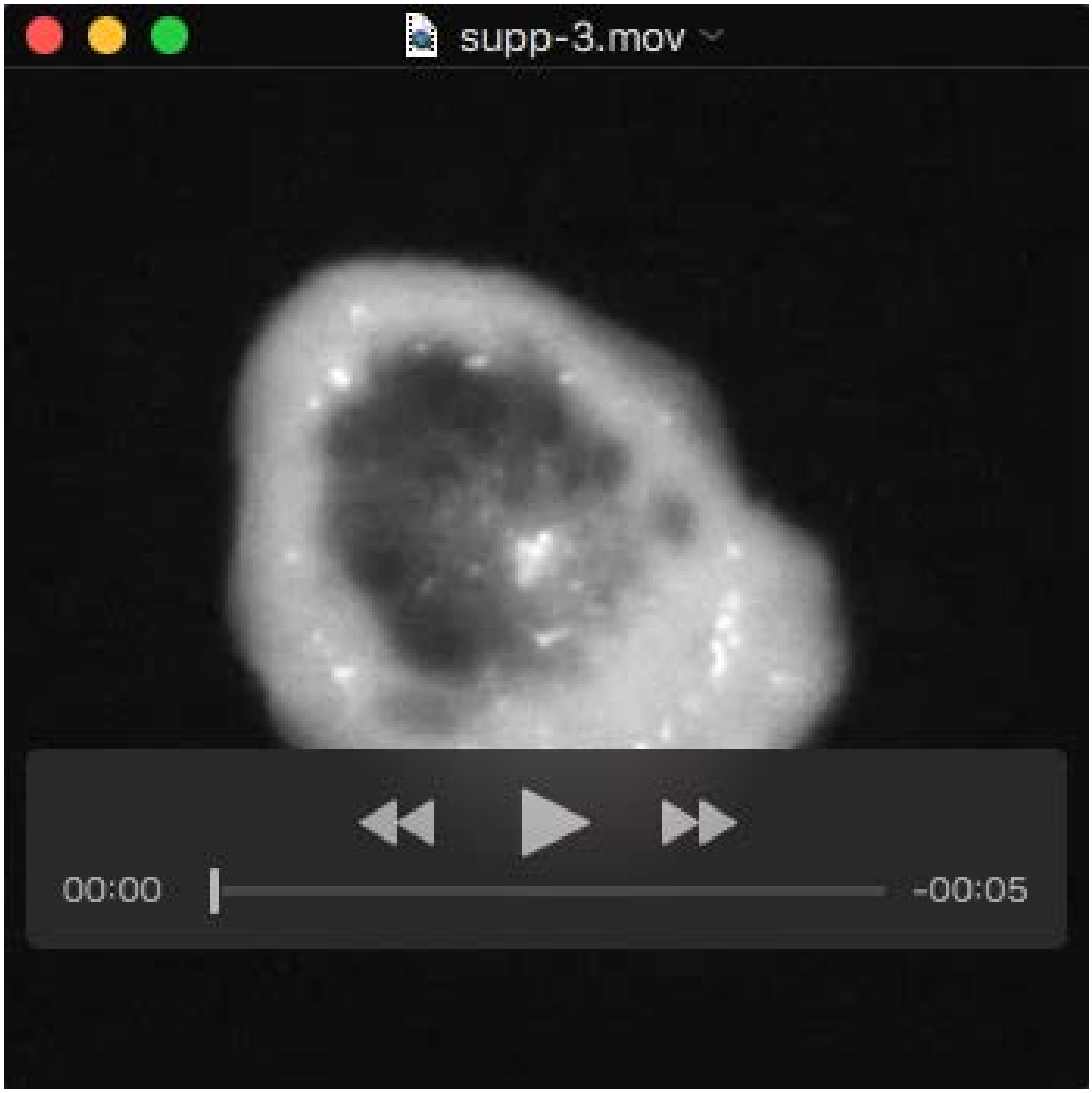

Movie S2. The SLP-76 SH2 domain regulates TCR-induced SLP-76 microcluster centralization and persistence (RK SLP-76 movie). SLP-76 deficient Jurkat T cells (J14 cells) were transiently transfected with an expression vector for an SH2 mutant (R448K; RK) SLP-76.YFP chimera of human origin.

Movie S3. The SLP-76 SH2 domain enables microcluster cohesion (WT STD movie #1). SLP-76 deficient Jurkat T cells (J14 cells) were transiently transfected with an expression vector for a wild-type (WT) SLP-76.YFP chimera of human origin. Magnification is 3x greater than in movies S1-2.

Movie S4. The SLP-76 SH2 domain enables microcluster cohesion (WT STD movie #2). SLP-76 deficient Jurkat T cells (J14 cells) were transiently transfected with an expression vector for a wild-type (WT) SLP-76.YFP chimera of human origin. Magnification is 3x greater than in movies S1-2.

Movie S5. The SLP-76 SH2 domain enables microcluster cohesion (RK STD movie #1). SLP-76 deficient Jurkat T cells (J14 cells) were transiently transfected with an expression vector for an SH2 mutant (R448K; RK) SLP-76.YFP chimera of human origin. Magnification is 3x greater than in movies S1-2.

Journal of Cell Science • Supplementary information

Movie S6. The SLP-76 SH2 domain enables microcluster cohesion (RK STD movie #2). SLP-76 deficient Jurkat T cells (J14 cells) were transiently transfected with an expression vector for an SH2 mutant (R448K; RK) SLP-76.YFP chimera of human origin. Magnification is 3x greater than in movies S1-2.

Journal of Cell Science • Supplementary information

Movie S7. The ADAP-120 and ADAP-130 isoforms both enter TCR-induced SLP-76 microclusters and lamellipodia (TRT control movie). J14.SY cells were transiently transfected with a 3xFlag.TRT control for the ADAP expression vectors seen in movies S8-S9. TRT protein is shown in the left panel and in red in the merge, SLP-76 in the middle panel and in green in the merge.

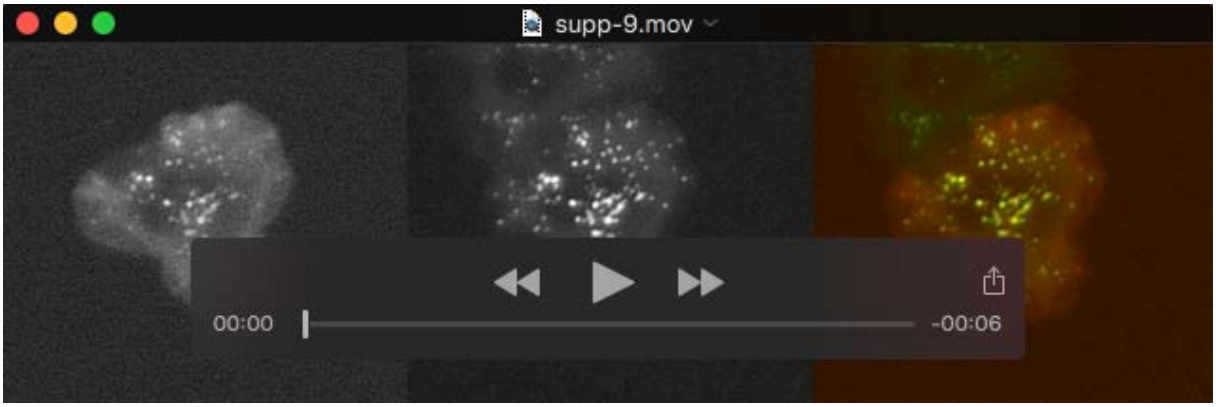

Movie S8. The ADAP-120 and ADAP-130 isoforms both enter TCR-induced SLP-76 microclusters and lamellipodia (ADAP-120 movie). J14.SY cells were transiently transfected with a 3xFlag.TRT.ADAP expression vector for ADAP-120. ADAP is shown in the left panel and in red in the merge, SLP-76 in the middle panel and in green in the merge.

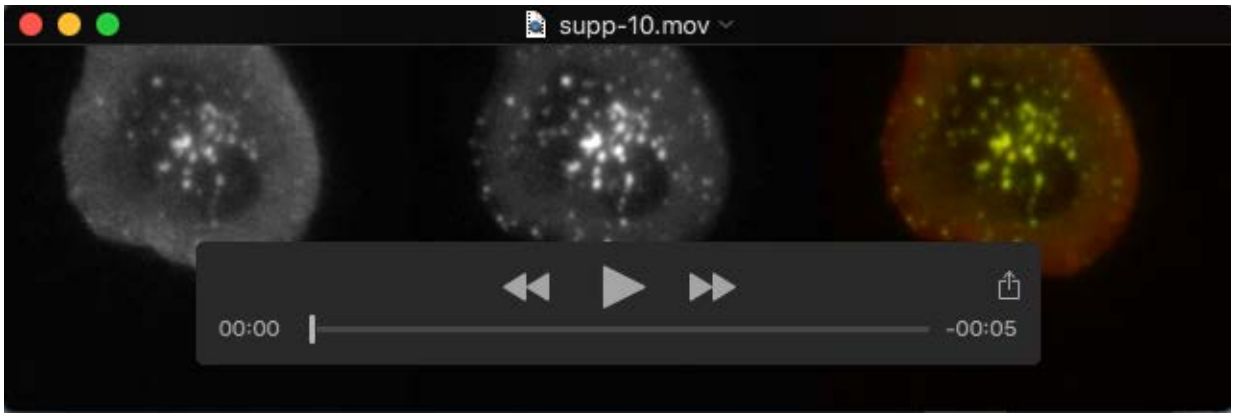

Movie S9. The ADAP-120 and ADAP-130 isoforms both enter TCR-induced SLP-76 microclusters and lamellipodia (ADAP-130 movie). J14.SY cells were transiently transfected with a 3xFlag.TRT.ADAP expression vector for ADAP-130. ADAP is shown in the left panel and in red in the merge, SLP-76 in the middle panel and in green in the merge.

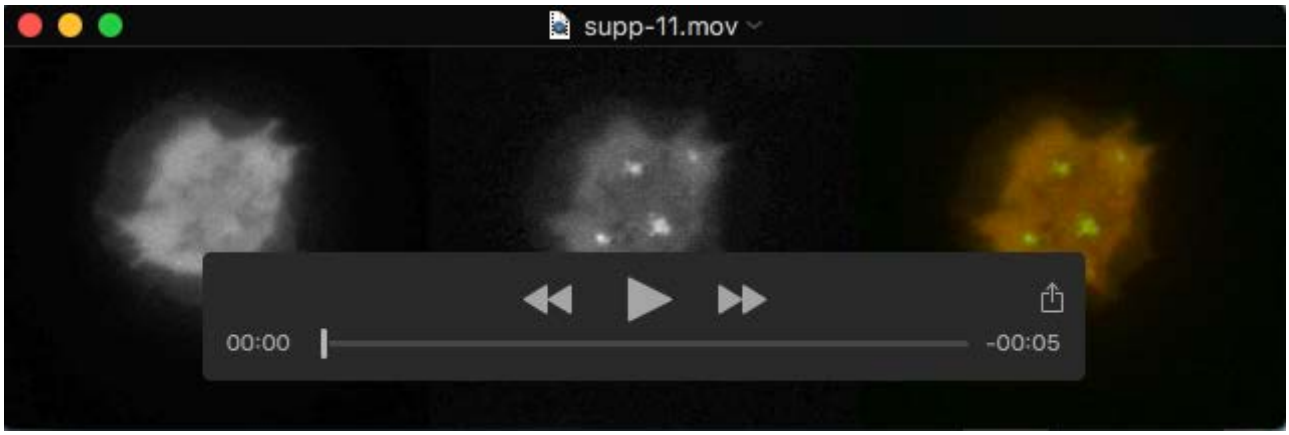

Movie S10. ADAP enhances the persistence and movement of TCR-induced SLP-76 microclusters (ADAP KD movie). J14.SY cells were transiently transfected with a dual expression vector encoding an shRNA specific for the 3'UTR of ADAP and a 3xFlag.TRT marker (ADAP KD). TRT protein is shown in the left panel and in red in the merge, SLP-76 in the middle panel and in green in the merge.

Movie S11. ADAP enhances the persistence and movement of TCR-induced SLP-76 microclusters (ADAP KD/AB movie). J14.SY cells were transiently transfected with a dual expression vector encoding an shRNA specific for the 3'UTR of ADAP and a 3xFlag.TRT.ADAP-120 chimera (ADAP KD/AB). ADAP was expressed at near endogenous levels, as confirmed in Figure 2A. ADAP is shown in the left panel and in red in the merge, SLP-76 in the middle panel and in green in the merge.

Movie S12. The overexpressed C-terminal fragment of ADAP antagonizes SLP-76 microcluster persistence and movement via phosphotyrosine-dependent interactions (WT C-term movie). J14.SY cells were transiently transfected with an expression vector encoding a 3xFlag.TRT-tagged chimera of the wild-type C-terminal fragment of ADAP-120. ADAP is shown in the left panel and in red in the merge, SLP-76 in the middle panel and in green in the merge.

Journal of Cell Science • Supplementary information

Movie S13. The overexpressed C-terminal fragment of ADAP antagonizes SLP-76 microcluster persistence and movement via phosphotyrosine-dependent interactions. (Y595F C-term movie) J14.SY cells were transiently transfected with an expression vector encoding a 3xFlag.TRT-tagged chimera of the Y595F mutated C-terminal fragment of ADAP-120. ADAP is shown in the left panel and in red in the merge, SLP-76 in the middle panel and in green in the merge.

Journal of Cell Science • Supplementary information

Movie S14. ADAP enters cytoskeletal contact structures prior to the recruitment of SLP-76. J14.SY cells were transiently transfected with ADAP knockdown-addback vectors as in movies S10-11. A representative cell was captured during its first moments of contact with the stimulatory cover slip. ADAP is shown in the left panel and in red in the merge, SLP-76 in the middle panel and in green in the merge. Note that ADAP is enriched in protrusive structures before SLP-76 is recruited into the contact, that SLP-76 microclusters form at the tips of these projections, and that ADAP enters the nascent microclusters concurrently with SLP-76.

Movie S15. The SLP-76 SH2 domain is dispensable for the transient enrichment of ADAP into contact structures (TRT.ADAP with mYFP). J14 cells were transiently co-transfected with 3xFlag.TRT.ADAP-120.WT and mYFP expression vectors. ADAP is shown in the left panel and in red in the merge, mYFP in the middle panel and in green in the merge.

Movie S16. The SLP-76 SH2 domain is dispensable for the transient enrichment of ADAP into contact structures (TRT.ADAP with SLP-76.WT.mYFP). J14 cells were transiently co-transfected with 3xFlag.TRT.ADAP-120.WT and SLP-76.WT.mYFP expression vectors. ADAP is shown in the left panel and in red in the merge, mYFP in the middle panel and in green in the merge.

Movie S17. The SLP-76 SH2 domain is dispensable for the transient enrichment of ADAP into contact structures (TRT.ADAP with SLP-76.RK.mYFP). J14 cells were transiently co-transfected with 3xFlag.TRT.ADAP-120.WT and SLP-76.RK.mYFP expression vectors. ADAP is shown in the left panel and in red in the merge, SLP-76 in the middle panel and in green in the merge. Note that ADAP is enriched in the lamellipodia formed in the presence of the SH2 domain-mutated SLP-76 chimera. ADAP also forms labile 'patches' in the absence of a functional SLP-76 SH2 domain.

Journal of Cell Science • Supplementary information